

UNCLASSIFIED

AD NUMBER

ADB013307

LIMITATION CHANGES

TO:

Approved for public release; distribution is unlimited.

FROM:

Distribution authorized to U.S. Gov't. agencies only; Proprietary Information; JUN 1976. Other requests shall be referred to Naval Surface Weapons Center, Attn: WOL, Code W-R-43, White Oak, Silver Spring, Maryland 20910.

AUTHORITY

USNSWC ltr, 3 sep 1982

THIS PAGE IS UNCLASSIFIED

L

NSWC/WOL/TR 76-58 ✓

②

NSWC/WOL/TR 76-58

NSWC

TECHNICAL REPORT

WHITE OAK LABORATORY

AD B O I 3 3 0 7

SPVD MAGNETIC SENSOR DEVELOPMENT

BY
J.F. Scarzello
G.W. Usher

JUNE 1976

NAVAL SURFACE WEAPONS CENTER
WHITE OAK LABORATORY
SILVER SPRING, MARYLAND 20910

Distribution limited to U.S. Government agencies only; Proprietary Information. Date statement applied June 1976. Other requests for this publication must be referred to NSWC/WOL, Code WR-43.

AD NO. _____
DDC FILE COPY

DDC
RECEIVED
SEP 18 1976
B

NAVAL SURFACE WEAPONS CENTER
WHITE OAK, SILVER SPRING, MARYLAND 20910

UNCLASSIFIED

SECURITY CLASSIFICATION OF THIS PAGE (When Data Entered)

REPORT DOCUMENTATION PAGE		READ INSTRUCTIONS BEFORE COMPLETING FORM
1. REPORT NUMBER NSWC/WOL/TR-76-58	2. GOVT ACCESSION NO.	3. RECIPIENT'S CATALOG NUMBER
4. TITLE (and Subtitle) SPVD Magnetic Sensor Development	5. TYPE OF REPORT & PERIOD COVERED Jan 76 - June 76	
7. AUTHOR(s) J. F. Scarzello, G. W. Usher	6. PERFORMING ORG. REPORT NUMBER	
9. PERFORMING ORGANIZATION NAME AND ADDRESS Naval Surface Weapons Center White Oak Laboratory White Oak, Silver Spring, Maryland 20910	8. CONTRACT OR GRANT NUMBER(s) FHWA ORDER NUMBER 6-3-0063	
11. CONTROLLING OFFICE NAME AND ADDRESS	12. REPORT DATE June 76	10. PROGRAM ELEMENT, PROJECT, TASK AREA & WORK UNIT NUMBERS
14. MONITORING AGENCY NAME & ADDRESS (if different from Controlling Office)	13. NUMBER OF PAGES 64	15. SECURITY CLASS. (of this report) UNCLASSIFIED
16. DISTRIBUTION STATEMENT (of this Report) Distribution limited to U.S. Government Agencies only; Proprietary Information. Date statement applied June 1976. Other requests for this publication must be referred to NSWC/WOL, Code WR-43.		
17. DISTRIBUTION STATEMENT (of the abstract entered in Block 20, if different from Report)		
18. SUPPLEMENTARY NOTES This research was sponsored by the Federal Highway Administration, Office of Research, Traffic Systems Division, Washington, D. C. 20590.		
19. KEY WORDS (Continue on reverse side if necessary and identify by block number) Magnetometer, Low power magnetic sensor, Two axis magnetometer, Brown Magnetometer, gradiometer, vehicle detection		
20. ABSTRACT (Continue on reverse side if necessary and identify by block number) Development of a low power Brown type ring core magnetometer is described for a Self Powered Vehicle Detector (SPVD) unit capable of sensing motor vehicles in a roadway. Sensor stabilization techniques are discussed and a digital feedback loop designed for improving magnetometer performance and sensor logic functions. The optimized sensor with digital feedback stabilization and low power logic appears adequate for the SPVD.		

DD FORM 1473 1 JAN 73

EDITION OF 1 NOV 65 IS OBSOLETE
S/N 0102-014-6601

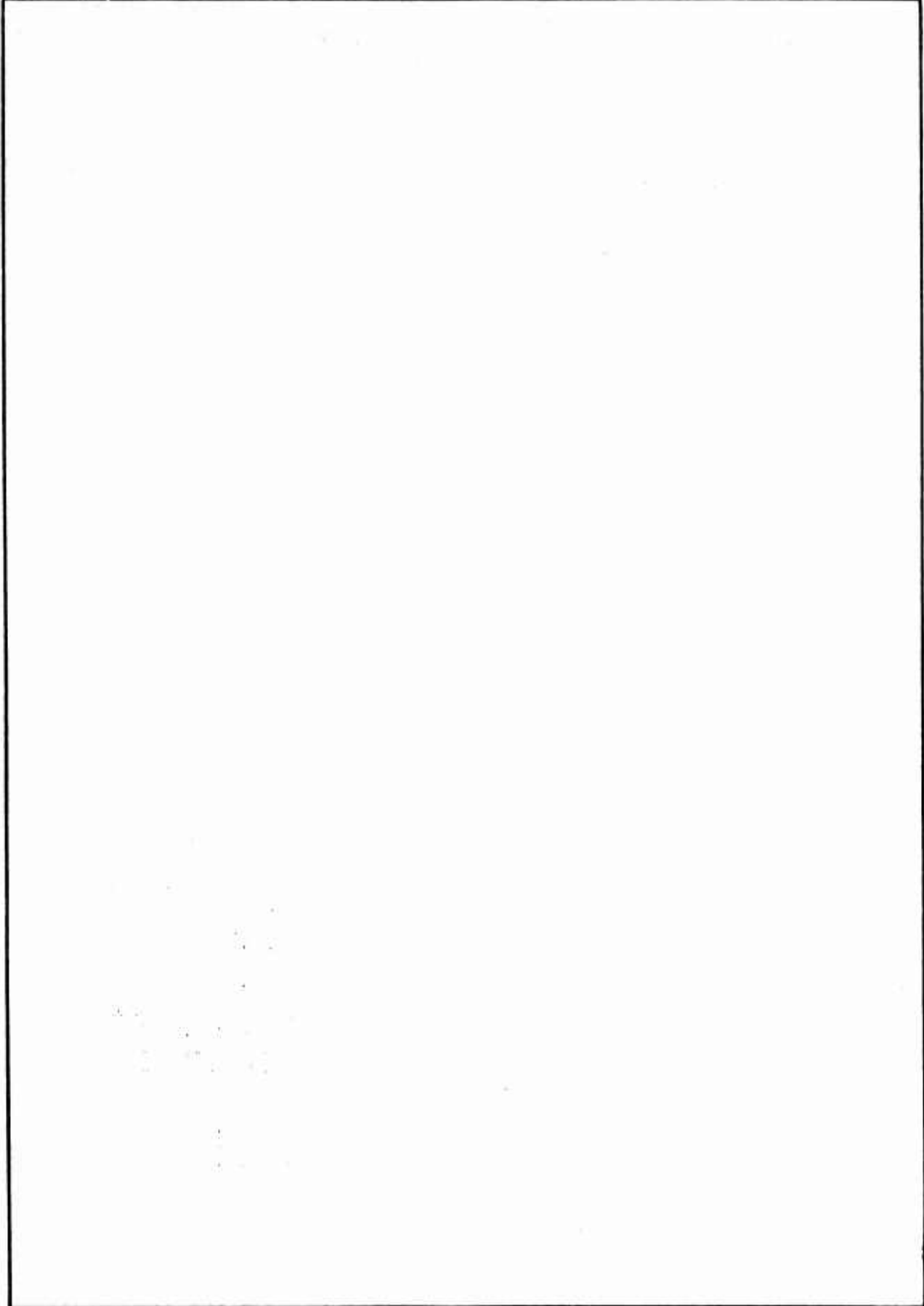
UNCLASSIFIED

SECURITY CLASSIFICATION OF THIS PAGE (When Data Entered)

391 596

VB

SECURITY CLASSIFICATION OF THIS PAGE(When Data Entered)



SECURITY CLASSIFICATION OF THIS PAGE(When Data Entered)

June 1976

NSWC/WOL/TR 76-58

SPVD MAGNETIC SENSOR DEVELOPMENT

This report documents the work performed by the Naval Surface Weapons Center on optimizing a magnetic sensor for the Federal Highway Administration's self-powered vehicle detector (SPVD) program. The report covers the initial refinement of the self-powered vehicle detector in accordance with the Federal Highway Administration Intra-Government Order No. 6-3-0063 for the January to May 1976 period and fulfills the required program documentation. The authors gratefully acknowledge the contributions of Wayne R. Grine and Chester W. Purves to the program.



LEMMUEL L. HILL

ACCESSION FOR	
NTIS	White Section <input type="checkbox"/>
DDC	Buff Section <input checked="" type="checkbox"/>
UNANNOUNCED	<input type="checkbox"/>
JUSTIFICATION.....	
BY.....	
DISTRIBUTION/AVAILABILITY CODES	
Dist.	AVAIL. and/or SPECIAL
B	

TABLE OF CONTENTS

	Page
LIST OF TABLES	3
LIST OF FIGURES	4
I. INTRODUCTION	6
II. TWO AXIS BROWN MAGNETOMETER	9
III. GRADIOMETER APPROACH	23
IV. INTERFACE PROBLEM	30
V. HONEYWELL SENSOR	33
VI. DIGITAL FEEDBACK CIRCUIT	41
VII. DISCUSSION	63

LIST OF TABLES

Table	Title	Page
1	SPVD Sensor Technical Requirements	8
2	Low Power Two Axis Brown Magnetometer Specifications	17
3	Maximum Power Dissipation for an n-bit R-2R network	47
4	Minimum Time a Vehicle Must Remain Stopped as a Function of Peak Magnetic Field Signature	57

LIST OF FIGURES

Figure	Title	Page
1	Low Power Brown Magnetometer Schematic Diagram	10
2	Two Axis Brown Magnetometer	15
3	Core Winding Instructions	16
4	Dynamic Range Plot of Two Axis Brown Magnetometer	20
5	Two Axis Magnetometer Temperature Performance	21
6	Magnetic Gradiometer Schematic	24
7	Gradiometer Temperature Performance	26
8(a)	Gradiometer Vehicle Signatures	27
8(b)	Gradiometer Vehicle Signatures	28
9	Modified SPVD Sensor Board Schematic	32
10	Flyback Voltage vs Pulse Width	34
11	Core Drive Circuit and Associated Waveforms	34
12	Honeywell Voltage Controlled Oscillator	36
13	VCO Waveforms	36
14	Inverter diagram	37
15	VCO Inverter Illustrative Schematic	37
16	Block Diagram, Honeywell Analog Feedback Circuit	42
17	Block Diagram, Digital Feedback Circuit	42
18	Digital Feedback Circuit Schematic Diagram	43
19	Four BIT R-2R Network	45
20	Power Dissipation vs Number of Bits for an R-2R Network	45
21	SPVD Logic Block Diagram	52

LIST OF FIGURES (CONT.)

Figure	Title	Page
22	Magnetometer Output vs Stopped Vehicle Presence Time	55
23	Schematic Diagram of Digital Feedback and Interface Circuits for Use With the Brown Magnetometer	59
24	Block diagram of Digital Feedback and Interface Circuits for Use With the Brown Magnetometer	61

I. INTRODUCTION

The Naval Surface Weapons Center, White Oak Laboratory, was introduced to the Federal Highway Administration vehicle detection problem in August 1975 when personnel of both facilities met to discuss the work documented in reference (1). In January 1976 a modest program was established at NSWC/WOL to optimize the self-powered vehicle detectors (SPVD) magnetic sensor.

The purpose of the SPVD is to reliably detect vehicles passing through a desired surveillance zone (traffic lane) in all environments associated with its fixed location beneath the roadway. The detected information is then telemetered via RF link to a roadside monitoring station for vehicular counting or traffic control. Unit operational life is to be greater than one year utilizing its self-contained batteries.

Herein are the results of the NSWC investigation to optimize a magnetic sensor for vehicle detection. The program was directed to investigate these objectives: (a) the suitability of the low-power two-axis Brown magnetometer, (b) optimization of the existing sensor described in reference (1), and (c) briefly explore single and two-axis magnetic gradiometers.

(1) Wick, D.C., Lubke, R.A., Vehicle Detection, Phase 1, SPVD Development (U) Report No. FHWA-RD-75-18, Jan 1975 (U).

The main problem addressed is stopped vehicle detection. The stopped vehicle presence may be addressed in two ways, i.e., having a magnetic sensor capable of responding to large long-term changes in field or by employing a gradiometer sensor. Engineering details of this investigation are documented herein. Sensor technical requirements are tabulated in Table 1.

TABLE 1

SPVD SENSOR TECHNICAL REQUIREMENTS

1. Detection Range Speed: 0 to 128 Km/hr (0 to 80 mph) 35.6 m/sec.
(117 ft/sec)
2. Detection Output: Pulse output for leading and trailing edge
of vehicle.
3. Detection Range: (Lateral from lane centerline)
 - Cars: $\pm 1.2\text{m}$ (± 4 ft)
 - Trucks: $\pm 1.2\text{m}$ (± 4 ft)
 - Buses: $\pm 1.2\text{m}$ (± 4 ft)
 - Motorcycles: $\pm .6\text{m}$ (± 2 ft)
4. Power Consumption: < 300 ua at 6.0v (1.8 mw)
5. Operating Temperature: -34°C to $+76^{\circ}\text{C}$ (-30°F to $+170^{\circ}\text{F}$)
6. Maximum Vehicle Counts: 20,000/day
7. Operating Lifetime: Minimum 1 year
8. Dimension: 7.62cm (3") dia x 15.24cm (6") long (sensor)
9. Sensor frequency response: 0 Hz to 40 Hz
10. Sensor DC Offset: $< \pm 50$ mv
11. Sensitivity: 28.5 mv/nT: (.9 mv/nT.) 1 V out for 7000 nT with
5% linearity for stated dynamic range
12. Sensor dynamic range: $\pm .7 \times 10^{-4}$ Tesla ($\pm .7$ oersted)

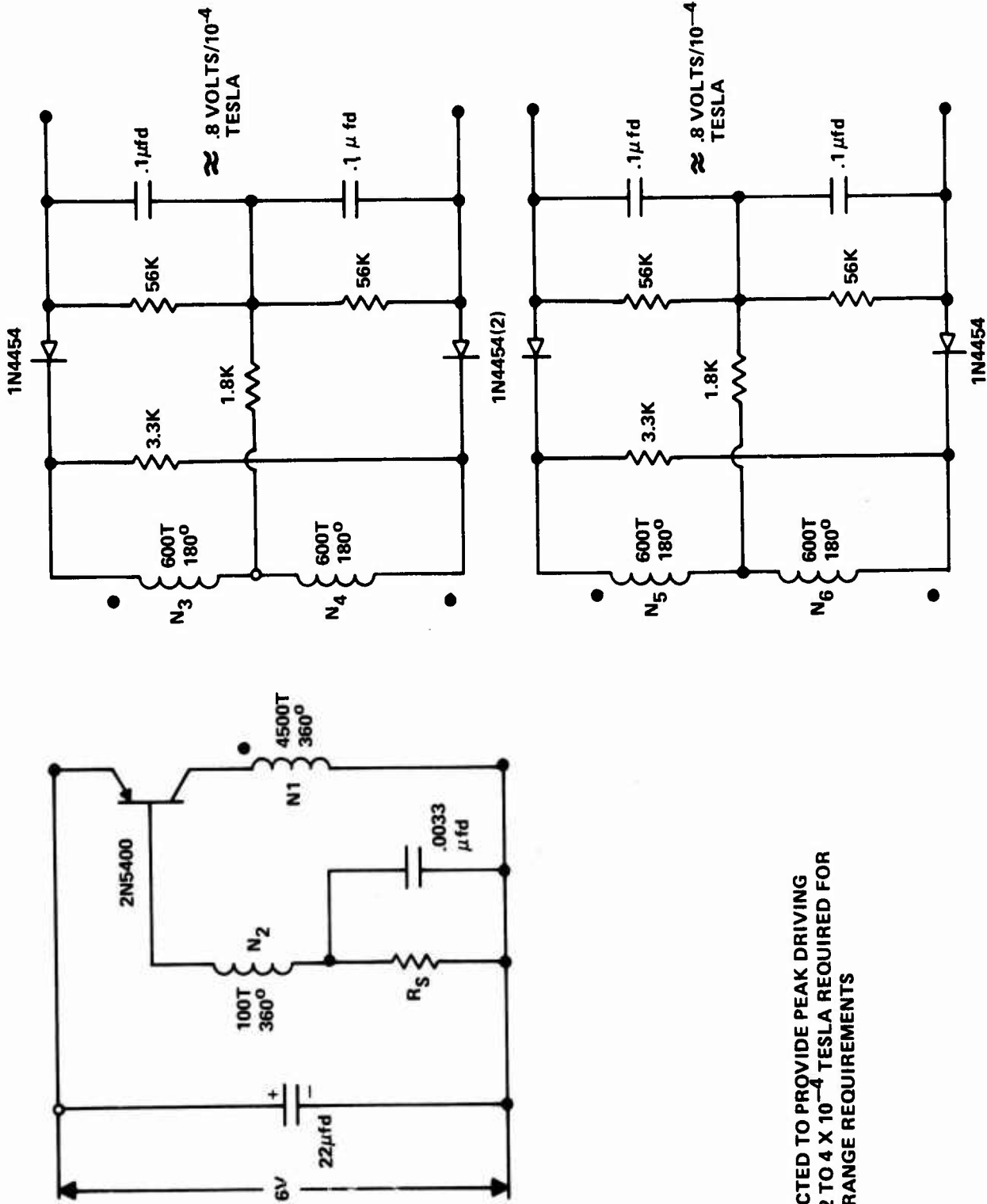
II. THE TWO AXIS BROWN MAGNETOMETER

General

The Brown magnetometer^{2,3,4,5} was originally developed for the Navy Vietnam Laboratory Assistance Program's (VLAP) NBB/MID tactical magnetic surveillance sensor as a miniature, low-cost and low-power magnetometer. This device has been used in numerous surveillance sensors and other devices since 1969.

The Brown-type fluxgate magnetometer employs a small permalloy tape bobbin core which may be purchased commercially from Infinetics, Inc., Wilmington, Delaware, Part No. S625C31-HC-2074C. Other manufacturers are also capable of supplying this core. The core consists of ten wraps of .03 mm (1/2 mil) thick, 4-79 permalloy tape .16 cm (1/16") wide on a stainless steel bobbin of nominal 1.6 cm (5/8") diameter. A magnetically coupled drive oscillator and detection circuit schematic is shown in Fig. 1. Windings N_1 and N_2 are wound 360° around the core. N_3 and N_4 are wound on opposite 180° segments of the core (in single-axis sensor) and are connected together to cancel the drive signal. For the two-axis magnetometer, N_3 , N_4 and N_5 , N_6 are wound on opposite 90° segments and connected

- (2) J. F. Scarzello, R.E. Brown and J.F. Haben, "NBB/MID, A Magnetic Intrusion Detector," (U), Naval Ordnance Laboratory NOLTR 71-12, Jan. 1971, Confidential.
- (3) R. E. Brown, "A Miniature Fluxgate Magnetometer with Subgamma Noise," presented at the IEEE INTERMAG Conference, Kyoto, Japan, April 1972. (U)
- (4) R. E. Brown, "Magnetic Field Gradiometer Utilizing a Pair of Cores Driven by a Blocking Oscillator," U. S. Patent 3,649,908, 14 Mar 1972.
- (5) J. F. Haben and J. F. Scarzello, "Law Enforcement Applications of Magnetic Sensors," Proceedings 1972 Carnahan Conference on Electronic Crime Countermeasures, University of Kentucky, Lexington, KY, UKY-98, April 1972. (U)



R_S IS SELECTED TO PROVIDE PEAK DRIVING FIELD OF 2 TO 4 X 10⁻⁴ TESLA REQUIRED FOR DYNAMIC RANGE REQUIREMENTS

FIG. 1 (U) LOW POWER BROWN MAGNETOMETER SCHEMATIC DIAGRAM (U)

to form two perpendicular field-sensitive axes. The transistor (2N5400) acts as a switch to apply the battery voltage periodically without reversal of the induction. This minimizes drive power. Power consumption of a typical sensor (single or two-axis) is less than 5 milliwatts when low noise performance (.25nT pp) is desired. (1 nanotesla (nT) = 1 gamma; 10^5 nT = 1 oersted = 10^{-4} tesla).

The split magnetic field sense windings are wound on opposite 90° segments of the core (180° single-axis case) in such a way that the drive signal is canceled out in the two sets of windings and only the ambient two-axis field-dependent signals remain. Following saturation of the core, the transistor turns off, induction returns rapidly to an equilibrium point, and a large fly-back voltage spike appears on all windings. It is during this fly-back interval that the diodes in the detection circuit conduct and sample the ambient field signals in the two sets of sense windings. The fly-back path of the circuit is controlled largely by passive circuit elements. The low intrinsic noise observed in the magnetometer is due to detecting during the fly-back interval when the drive circuit is relatively quiescent.

The detection circuit for each axis consists of two diodes biased so that only the fly-back voltage spike from the two 90° sensor windings (per axis) is detected as a field-dependent signal polarity. The intrinsic noise of the magnetometer when operated at 5 milliwatts is less than .25 nanotesla peak to peak in the passband of .01 to 3 Hz for a temperature range of -29°C to +55°C

(-20°F to +130°F) and will operate at -40°C with less than .5 nanotesla peak-to-peak noise. The output circuit sensitivity is 25 microvolts/nanotesla and varies approximately 5% for $\pm 6 \times 10^{-4}$ tesla (± 6 oersted) applied field.

The magnetometer requires a low internal impedance power supply. The reason is that the sensor drive winding impedance drops sharply as the core saturates and there is a large drive current demand at this point. Using a large value tantalum capacitor across the battery or power supply produces a low impedance at the core drive frequency. The magnetometer has been optimized to operate on several supply voltages. A sensor designed to operate at some voltage, for example 4.05 volts will also operate on as low as 3 volts. Low temperature operation requires the use of a large tantalum capacitor across the battery, as the battery's internal impedance increases at low temperatures.

If the magnetometer is used with an amplifier having a power supply common to the drive supply, isolation between the drive and detection output portions of the magnetometer must be observed to preserve the magnetometers inherent low noise levels. Interwinding capacitances are involved in the magnetometer operation, especially during the critical fly-back portion of the drive cycle, and they must not be directly shorted out by connecting either terminal of the output circuit to the power supply terminals. There should be at least 10 K Ω of resistance between either output terminal and either side of the power supply.

The magnetometer radiates a small amount of drive signal and this may be picked up by any high-gain sensor amplifier in close proximity. A simple resistor-capacitor filter is used to prevent this small amount of feed-through from upsetting the sensor amplifier.

The magnetometer operates best (low noise) when the peak drive current at 40KHz is adjusted for 10 milliamperes peak drive current when operated from a 4-volt battery. The permalloy bobbin core is wound on a toroidal core winding machine with AWG #36 HF (heavy Formvar insulated) copper wire. The two-axis magnetometer core is slightly more difficult to wind than the single-axis sensor because there are four separate sense windings each occupying a 90° segment of the core.

Several hundred 4-volt single-axis Brown magnetometers have been built by WOL with no known failure. The tactical magnetic surveillance sensor DT-(XWO-7A)/GSQ-180 in the sensor system AN/GSQ-180(V) uses the single-axis Brown magnetometer and is currently in production. The 150 unit pilot production cost is \$150 per sensor which includes the Brown magnetometer, amplifier, threshold detector, pulse generator, cable and rugged housing.

Sensor Optimization

To further reduce the sensor power, more turns were added to the drive winding in order to maintain the saturating drive field with a reduced current. In order to preserve the output sensitivity, more sense windings are required while necessitating a smaller wire

size (#40AWG) to reduce the filling factor from additional drive windings. This brute force optimization, however, provided a two-axis sensor powered by .72 mw from a 6 volt battery, with no appreciable increase in size or electronics complexity. The core winding, however, is more involved and is shown in Fig. 3. The resulting low power sensor specifications for that illustrated in Figs. 1, 2, and 3 are tabulated in Table 2.

The two-axis core shown in Fig. 2 and illustrated in Fig. 3 may be wound by following core winding instructions detailed below. An experienced technician had no problem winding these cores and several manufacturers produce similar toroidal core magnetic sensors.

Magnetic Core Winding Instructions

1. Wrap cores with teflon tape (≈ 4 mil thick) or mylar tape to insulate the stainless steel bobbin from the windings. (See Figure 3)
2. Put the windings N_1 , N_2 , N_3 , N_4 , N_5 and N_6 on in order, with N_1 first.
3. The winding sense must be maintained; that is, the core is not turned over during winding, or between windings.
4. Number 40 HF (Heavy Formvar) copper magnet wire is used on all windings.
5. Windings are layered on at about 800 turns per 360° layer. A winding or layer requiring less density is distributed over the 360° winding space.
6. Numbered tags mark the beginning of each winding, the lowest

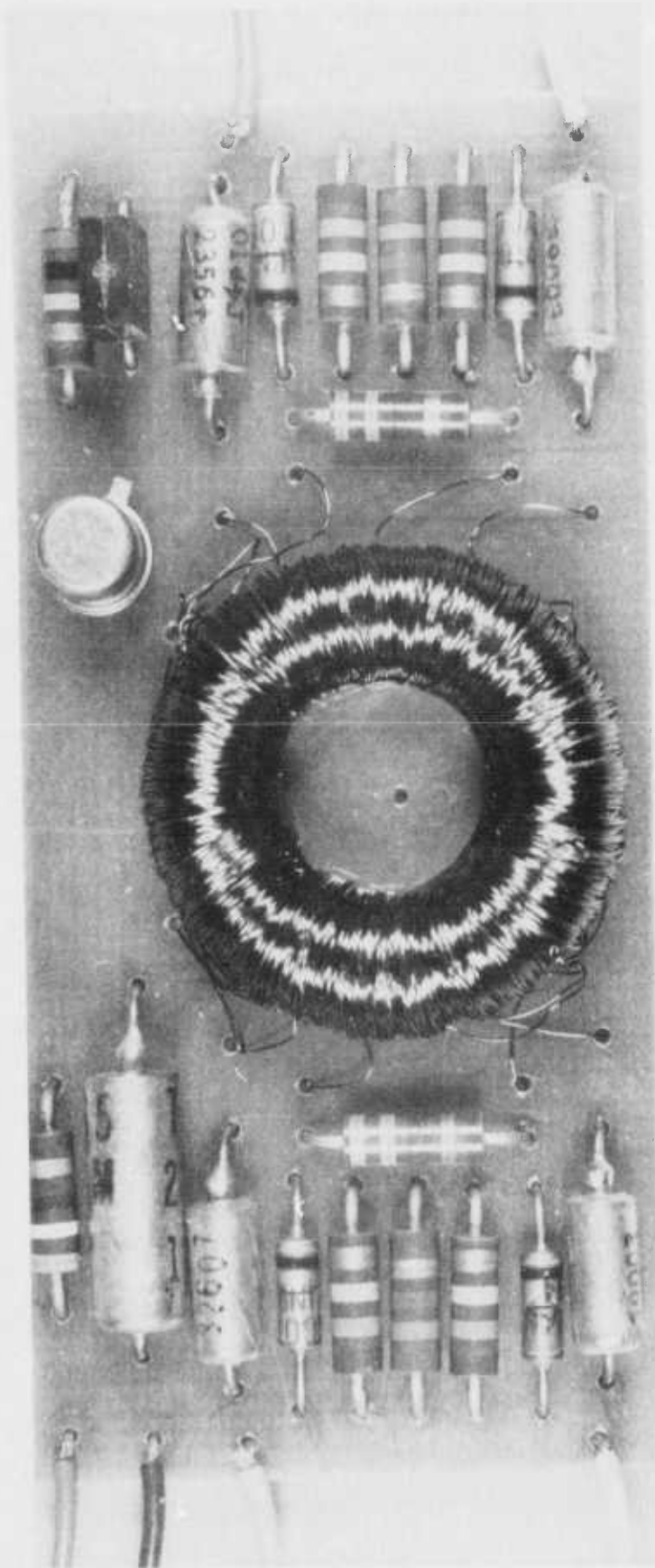
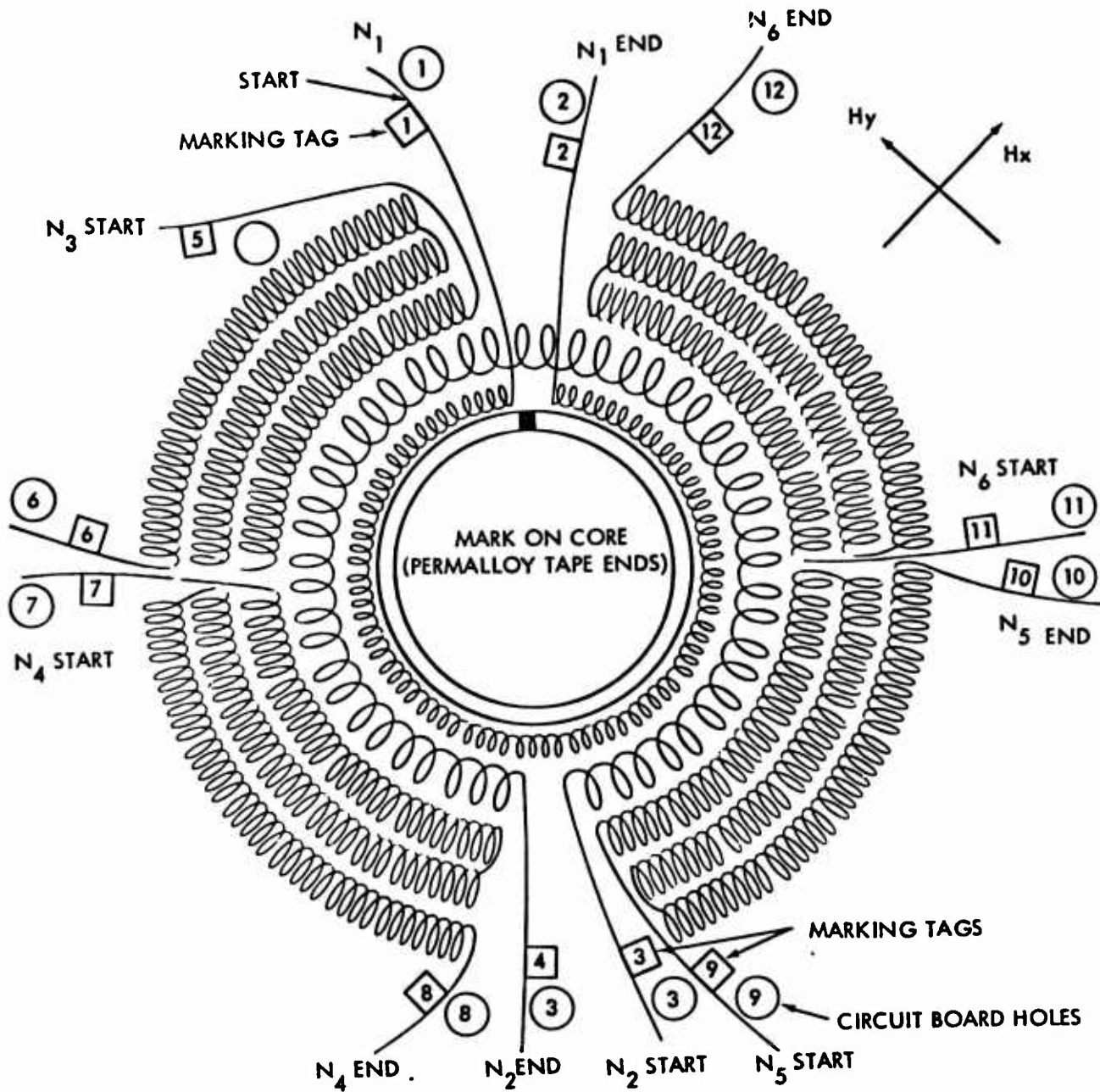


FIG. 2 (U) TWO-AXIS BROWN MAGNETOMETER (U)



$N_1 = 4500$ TURNS #40HF
 $N_2 = 100$ TURNS #40 HF
 $N_3 = N_4 = N_5 = N_6 =$
 600 TURNS #40HF

FIG. 3 CORE WINDING INSTRUCTIONS (U)

TABLE 2

LOW-POWER TWO-AXIS BROWN MAGNETOMETER SPECIFICATIONS

Sensitivity:	≈ 8 microvolts/nanotesla* (.8 volts/oersted)
Noise:	≈ 1.5 nanotesla, peak to peak (.01-3 Hz)*
Dynamic Range:	$.8 \times 10^{-4}$ tesla ($\pm .8$ oersteds)*
Linearity:	$\approx 5\% / \pm .8 \times 10^{-4}$ tesla)*
Power Consumption:	.72 milliwatts at 6.0 volts
Size:	4.76 cm x 3.0 cm x 1.27 cm (1 7/8" x 1 3/16" x 1/2")
Weight:	19 grams (.68 ounce)
Operating Temp:	-40°C to +70°C (-40°F to 158°F)

*Same for both x and y axes

number tag for start of winding N_1 to the highest number tag marking the starting lead of winding N_6 .

7. There are six windings required: the first, $N_1 = 4500$ turns is distributed around the core ~ 450 turns per layer for ten layers.

Leave a 5-inch length of wire on each end of the winding and on the starting wire put tag #1. At the end of this winding twist the wires together opposite the mark on the core where the winding was started, and mark with tag #2.

8. The second winding $N_2 = 100$ turns is started 180° opposite the start of winding N_1 . Mark the start lead (tag #3) and distribute the 100 turns evenly 360° and twist the wires together at the end of this winding. Mark the lead starting this winding with tag #3 and its end with tag #4.

9. N_3 is a 600-turn winding distributed evenly (~ 200 turns per layer for 3 layers) over one quarter (90°) of the core on one quarter of the side between the termination of windings N_1 and N_2 . Again mark the starting lead with a number tag (#5) and finish lead with tag #6.

10. N_4 is another 600-turn winding located on the other quarter of the core in an opposite 90° segment. Again, mark the start with a number tag (#7) and distribute the wire on the 90° segment in ~ 3 layers each containing about 200 turns. Mark the end of this winding with tag #8. Winding N_3 and N_5 together define one axis.

11. N_5 and N_6 are wound as N_3 and N_4 on the two remaining 90° core segments. Tag numbers 9, 10, 11 and 12 mark the start and finish of winding N_5 and N_6 respectively.

During the sensor optimization, a variety of core windings were tried. The #36 AWG wire which is used in most sensor models was changed to #40, although good single-axis sensor results were obtained with it, winding problems for a two-axis core could not be overcome easily. The sensitivity is relatively low, i.e., $.8 \text{ v}/10^{-4} \text{ tesla}$, ($8 \text{ } \mu\text{v}/\text{nT}$) but sufficient for vehicle detection. The lowest sensor power obtained was $.56 \text{ mw}$ @ 6 volts with a $\pm 1 \times 10^{-4}$ tesla dynamic range. However, stability of the operating point probably requires the higher power ($> .72 \text{ mw}$) to reduce failure rates from core variations on those from different manufacturers. The dynamic range graph of the optimized sensor is shown in Fig. 4. This sensor was temperature cycled in a magnetic shield over the range of -40°C to $+70^{\circ}\text{C}$ by forcing cold nitrogen gas from liquid nitrogen and heated air into the sensor dewar located inside a three layer magnetic shield. The offset drift with temperature was quite severe for the low powered sensor and is plotted in Fig. 5. The temperature was changed quite rapidly i.e., both temperature extremes were tested in less than 6 hours. Normal Brown type magnetometers have $\text{nT}/^{\circ}\text{C}$ drift or much less than that shown in Fig. 5. Three sensors were constructed with similar electrical/magnetic performance characteristics. Numerous cores were wound to gain confidence in the stability of sensor performance and to optimize design. Several wire sizes and number of turn combinations were tried, and consistently low powers were obtained in the order of 1 mw and with different transistors at the 6 volt power supply level.

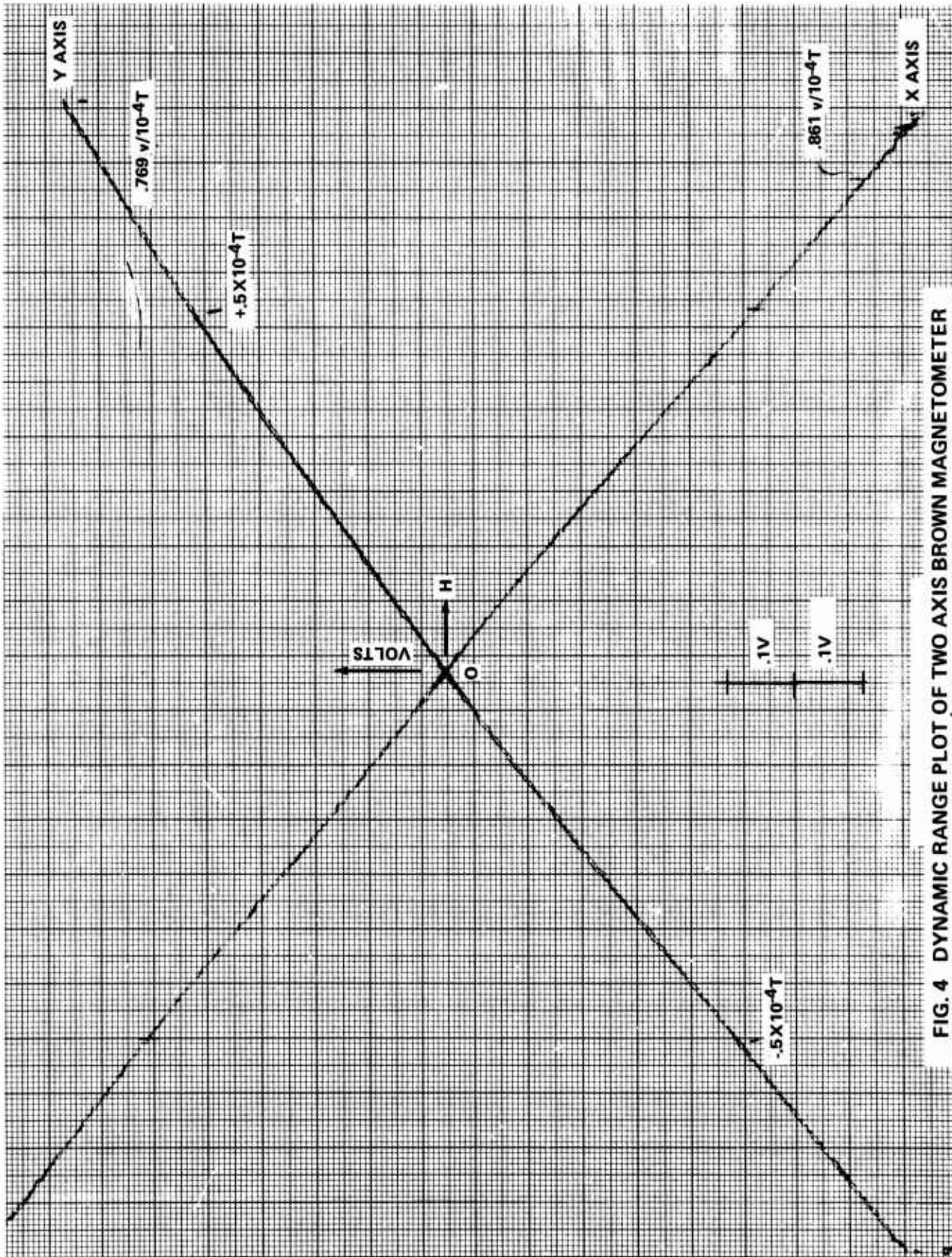


FIG. 4 DYNAMIC RANGE PLOT OF TWO AXIS BROWN MAGNETOMETER

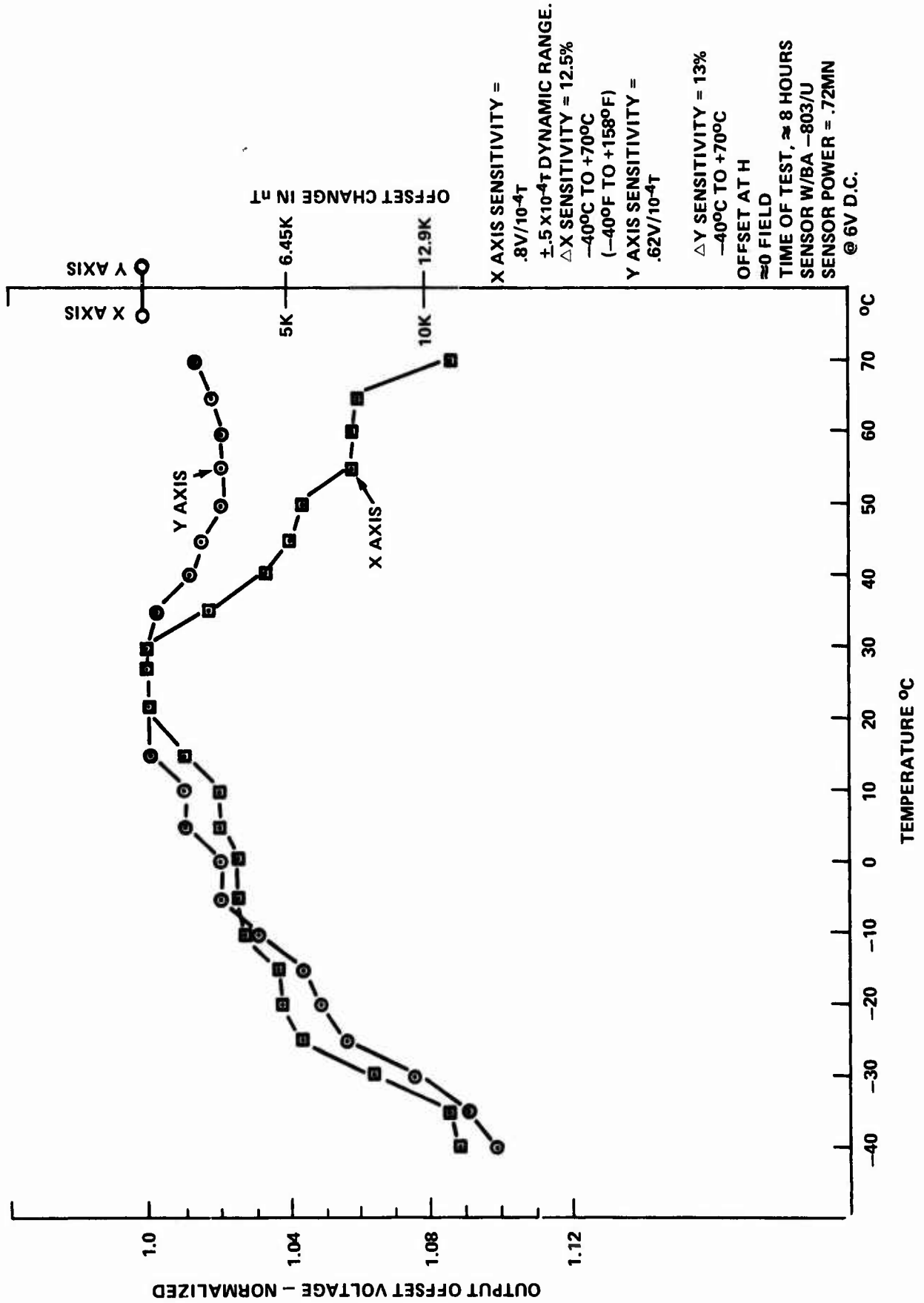


FIG. 5 TWO AXIS MAGNETOMETER TEMPERATURE PERFORMANCE

For example, a core wound with 4500T #40 HF = N_1 , $N_2 = 100T$, $N_3 = N_4 = N_5 = N_6 = 800T$ and in the circuit of Fig. 1 is operable at .34 mw @ 6V with $\approx .2V/10^{-4}$ tesla (.24/oersted) sensitivity over a $\pm .5 \times 10^{-4}$ tesla (.5 oersted) dynamic range. However, at 1 mw the sensor performs well and is stable for any anticipated change in battery voltage/temperature or ambient field changes (i.e., linear to $\pm 5\%$ for ± 1 oersted) and has x and y axis sensitivities greater than .7 volts/oersted. One sensor of this design has been built and partially tested. (The larger dynamic range is considered desirable since the SPVD may be close to roadway steel reinforcing rods.)

The "DC" characteristics of the Infinitics core used (S625-C31-HC-2074C) were taken by wrapping a 250 turns #36HF pick-up winding on the core with a 10 turn #22 hook-up wire (drive winding) to obtain nominal 60 Hz core characteristics; $B_{max} = .73$ tesla (7300 gauss), $H_c = .628 \times 10^{-3}$ amp turn/meter (.050 oersted) and with a squareness ratio (B_r/B_m) of 0.88.

Cores having these normal characteristics should be satisfactory for magnetometer operation and can be purchased from two other manufacturers. It is interesting to note that the sensor self-noise in zero ambient field of these low power sensors is still low and in the order of 1-2 nT p-p.

In summary, a two-axis low-power sensor can be constructed utilizing the Brown type magnetometer to meet the existing power requirements for the SPVD.

III. GRADIOMETER APPROACH

A single-axis magnetic gradiometer⁴ unit was constructed to investigate vehicle signature characteristics and sensor power/sensitivity requirements for an SPVD sensor. A gradiometer, if stable and sensitive enough, would be a desirable solution for the stopped vehicle detection problem and provide additional information for vehicle classification. Basically, the magnetic gradient greater or less than the natural gradient of the roadway location could be detected. Sensor alignment would not be critical since it is stationary and could be "zeroed" in place if required.

Figure 6 is a schematic diagram of the single axis unit. It was built on two layered boards, one being a 1 cm thick 10 cm x 4 cm phenolic block with two core turntables whose centers are 8 cm apart. The cores can be easily changed and two gradient positions can be sensed, i.e., $\frac{dH_x}{dy}$ and $\frac{dH_y}{dy}$. An amplifier (Fig. 6) is built on a 10 cm x 4 cm circuit board and positioned directly over the turntable sensor block. The unit is powered by a BA-803/U carbon zinc 6 volt battery. The power consumption is normally 2 mw (1.2 mw for sensor). There is ample sensitivity to detect a variety of vehicles. Sensor and DC coupled amplifier stability with respect to temperature, however, is not as good as expected.

(4) R. E. Brown, "Magnetic Field Gradiometer Utilizing a Pair of Cores Driven by a Blocking Oscillator," U.S. Patent 3,649,908, 14 March 1972.

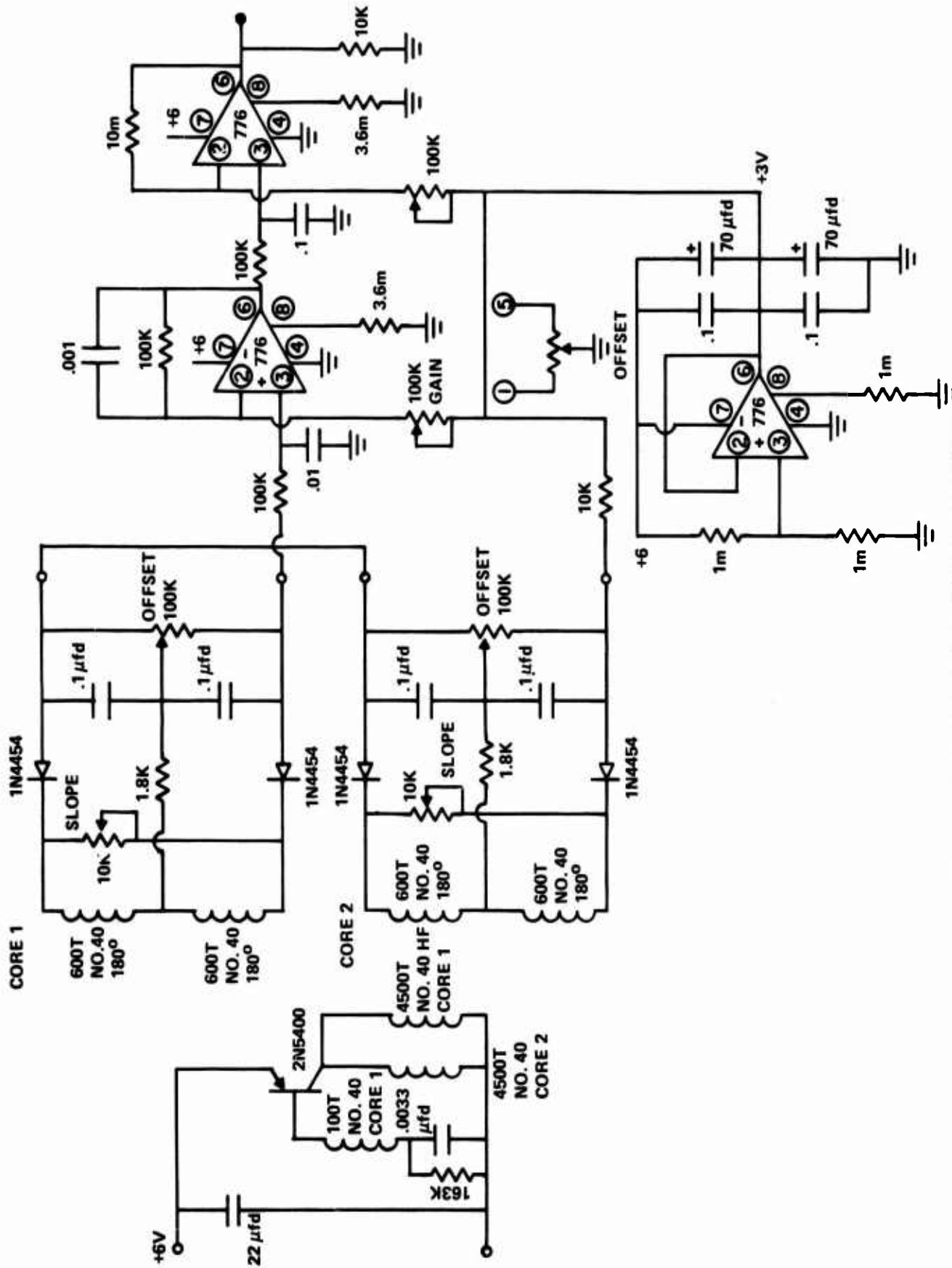


FIG. 6 MAGNETIC GRADIOMETER SCHEMATIC

Fig. 7 is a graph of the gradiometer temperature test results. The DC drift is about 900 nT for the -30°C to +70°C temperature range with a total change in sensitivity of 15%. Minor variations in sensor calibration current may be responsible for sensitivity changes and slight sensor movements inside the magnetic shield-dewar assembly will contribute to DC offset. These variations appear to be lower than vehicle signatures of interest (See Fig. 8).

The two gradiometer sensor cores may be wound with an additional sensor winding to make a two-axis gradiometer, i.e., dH_x/dy and dH_y/dy or capable of measuring 1st and 2nd gaussian gradient positions.

A magnetic gradiometer capable of sensing two gradients $\frac{dH_x}{dy}$ and $\frac{dH_y}{dy}$ was briefly used to determine vehicle magnetic signatures. It is constructed from two/dual-axis Brown magnetometers (standard 5mw sensors, total unit power consumption 14mw, with their output sensitivities matched and zero offset and alignment errors minimized. It was put in the NSWC roadway test hole, 12.7 cm (5") dia - 46 cm (18") deep with a phenolic liner and a 2.5 cm (1") thick 17.78 cm (7") diameter cover plate. A PVC non-magnetic waterproof test sensor housing 11.43 cm (4-1/2") diameter, 36.83 cm (14 1/2") long, with a 6-pin connector is used to monitor trial sensors. The sensor was adjusted to have the following sensitivity for a 9.5 cm gradient baseline.

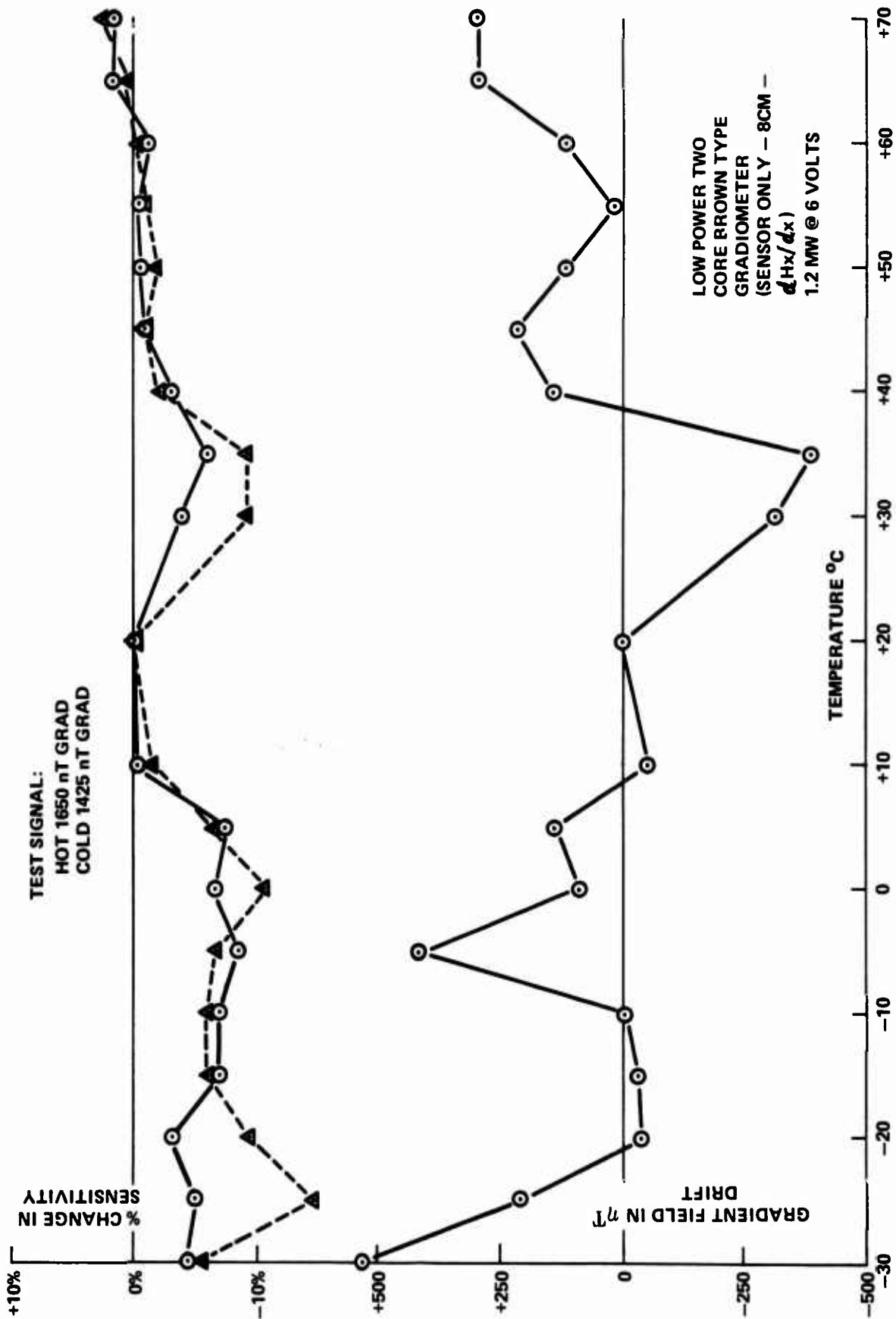


FIG. 7 GRADIOMETER TEMPERATURE PERFORMANCE

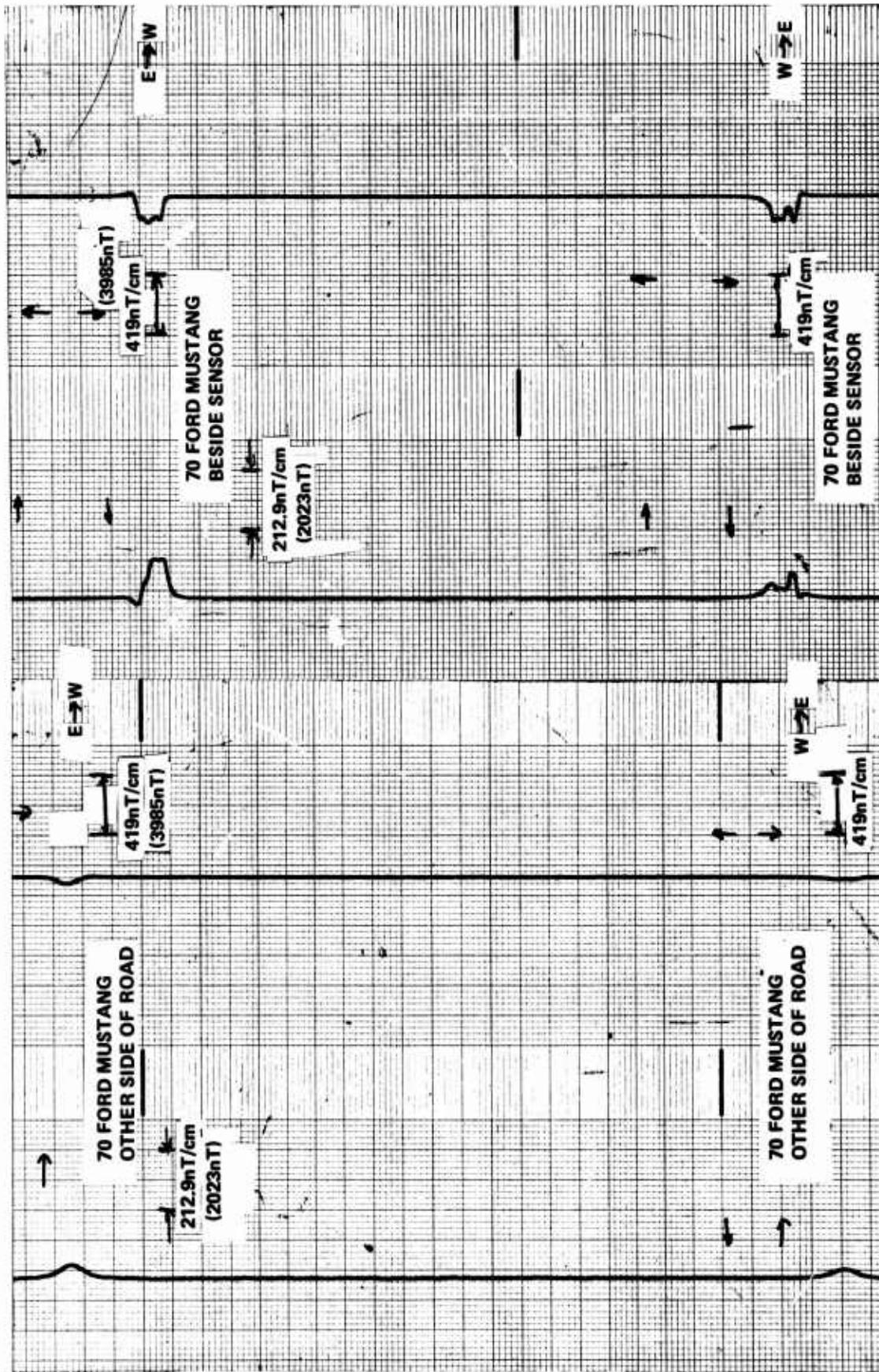


FIG. 8a GRADIOMETER VEHICLE SIGNATURES

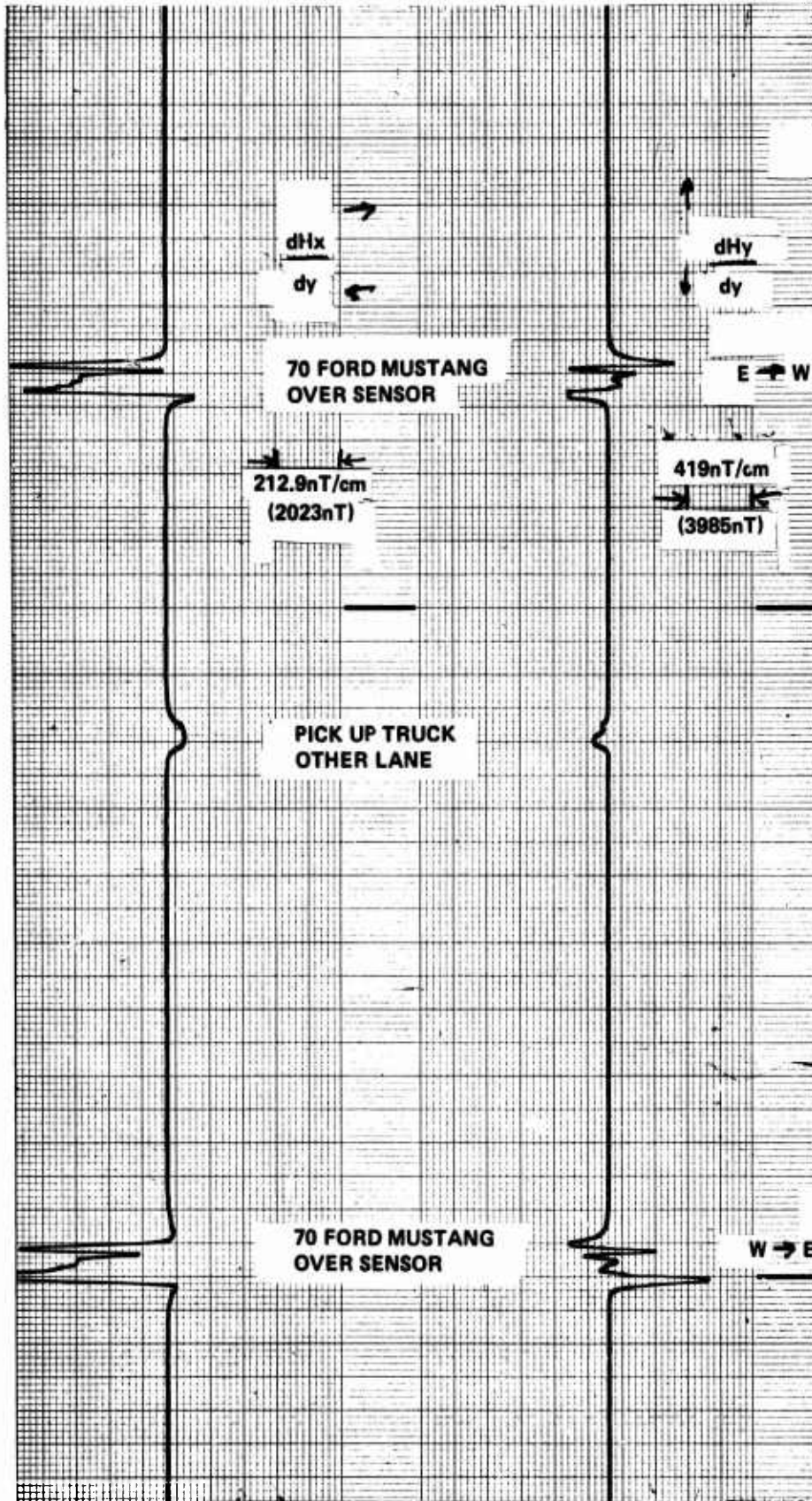


FIG. 8b GRADIOMETER VEHICLE SIGNATURES

$$\left. \frac{dH_y}{dy} \right|_{9.5\text{cm}} = 3985\text{nT/volt or } 419.5\text{nT. cm/volt}$$

$$\left. \frac{dH_x}{dy} \right|_{9.5\text{cm}} = 2023\text{nT/volt or } 212.9\text{nT. cm/volt}$$

A vehicle was driven past the emplaced sensor on an east-west heading resulting in order of magnitude signatures for a two-door 1970 Ford Mustang (8 cylinders). Fig. 8a and Fig. 8b are chart records showing signatures directly over and near the sensor. A very large gradient vehicle signature is observed in the order of hundreds of nT per centimeter gradient field.

IV. INTERFACE PROBLEM

The low-power two-axis Brown magnetometer described in the previous section is capable of sensing a vehicle but must be interfaced with appropriate electronics to amplify and process magnetometer signals. The sensor logic should not produce double vehicle counts for a single vehicle and reliably detect several types of motor vehicles, even when stopped in the sensors surveillance zone.

Logic previously developed required a vehicle signature whose characteristics are (1) initial detection when the signature amplitude exceeds 7000nT peak in the vertical axis, (2) detection is continued (i.e., vehicle is present) as long as the signal is greater than 3000nT in either vertical or horizontal sensor axis.

A sensitivity of 3500nT/volt (.28 5mv/nT) is required to interface a transducer to the existing electronics. The low power Brown magnetometer sensitivity $\approx .75 \text{ v}/10^{-4} \text{ tesla}$ requires amplification and appropriate coupling to remove the ambient field contribution to the electronics and to correct for any long term drifts associated with temperature or ambient field or component temporal variations.

A sensor board was fabricated containing a two-axis sensor with two low power amplifiers. Three interface approaches were considered, (a) capacitor coupled using large high quality polarized capacitors, (b) direct DC coupling by nulling the sensor offset when emplaced and (c) a digital feedback loop.

Since a fifteen minute (900 sec) presence time is desired, AC coupling requires an extremely high quality capacitor. Numerous capacitors were tried and some appeared good for several hours but its stability with respect to time and temperature were unacceptable. Large electrolytic capacitors (220 ufd) when properly polarized for long periods of time (2 weeks) appear to improve with respect to time and temperature drift (lower leakage currents).

Direct coupling the sensor by zeroing the unit in place was done to test the entire system with its modified logic and RF link to determine if any undesirable system interaction occurs. Fig. 9 is a schematic diagram of a modified sensor board replacing the two SPVD magnetometer boards.

This board was interfaced with the SPVD logic¹ which was modified by removing both sensor boards and putting the input of U14 (Pins 12 and 13) to +6 volts thereby disabling the stopped vehicle logic. The DC offset was nulled out using the offset pots (Fig. 9) and measured by a voltmeter on twisted hook-up wire with RF chokes. The unit works satisfactorily and can be operated without the sensor shield and not free run, but over a limited temperature range ($\approx 25^{\circ}\text{C}$).

The digital feedback loop system for the automatic ambient field zeroing and sensor stabilization with respect to time and temperature is the most desirable technique for sensor-logic interface. It is described in the next section.

(1) Wick, D.C., Lubke, R.A., Vehicle Detection, Phase 1, SPVD Development (U) Report No. FHWA-RD-75-18, Jan 1975 (U).

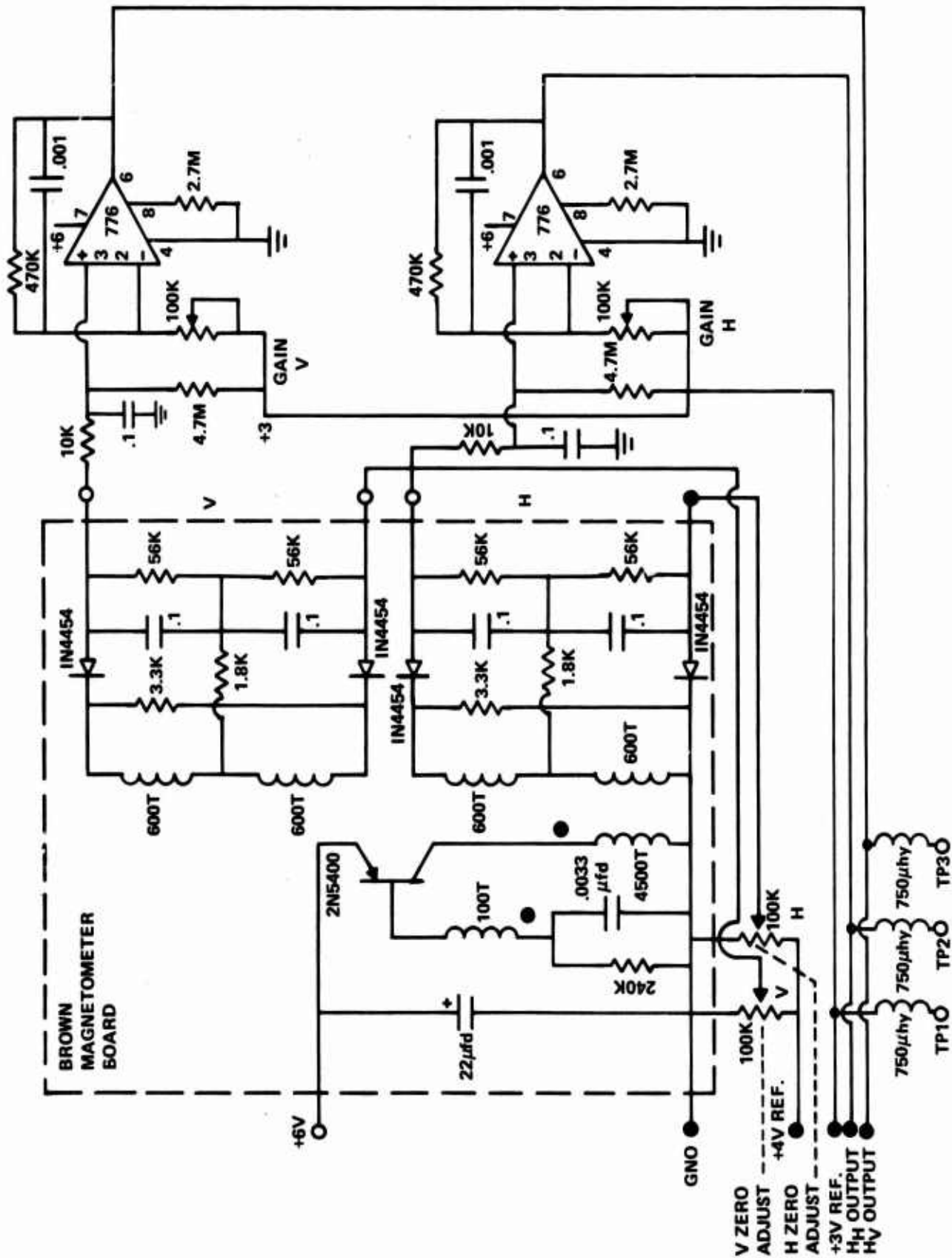


FIG. 9 MODIFIED SPVD SENSOR BOARD SCHEMATIC

V. HONEYWELL SENSOR

In order to determine exactly why the Honeywell sensor did not perform adequately, an analysis of its characteristics was attempted. A description of the operation of this sensor is given on page 32 of Ref. 1. It states that when the VCO turns on the drive transistor the "core is driven into a saturated state." Flyback voltage, developed when the drive pulse terminates, is detected and integrated by a diode-capacitor circuit to give a d-c output proportional to the ambient field change due to the detected vehicle.

Measurements of the Honeywell sensor voltages led to the conclusion that it is not driven into saturation by the drive pulse. If the core were driven into saturation, the flyback voltage should be independent of the pulse width. However, measurements of flyback voltage vs drive pulse width, as shown in figure 10, indicate a linear relationship between these two parameters. Figure 11 is a simplified schematic of the core, L1, and the drive circuitry. Figure 11a shows the voltage measured at the base of Q, and figure 11b shows the voltage actually measured at the collector of Q₁. V_f in figures 11b and 11c is the peak value of the flyback voltage. The voltage waveform of figure 11b also indicates that L1 does not saturate. Since L1 has a DC resistance of 124 ohms, and since its inductance drops to a small value during core saturation, the voltage at the collector of Q₁ should drop to a value dependent upon the dc resistance of the coil and the current through it. For the values shown in Figure 11, this voltage would have a magnitude of

(1) Wick, D.C., Lubke, R.A., Vehicle Detection, Phase 1, SPVD Development (U) Report No. FHWA-RD-75-18, Jan 1975 (U).

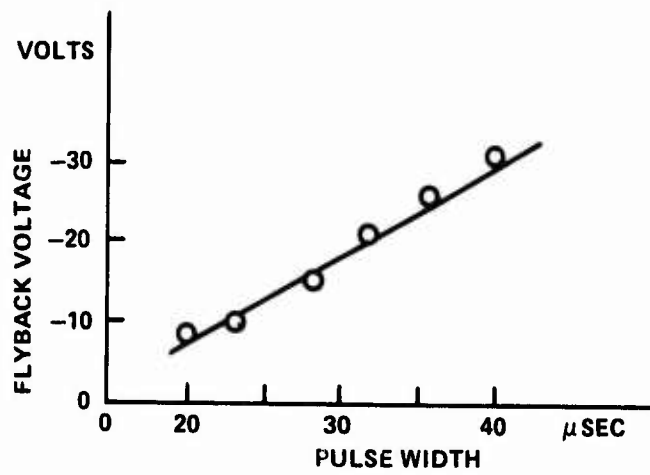


FIG. 10 FLYBACK VOLTAGE VS PULSE WIDTH

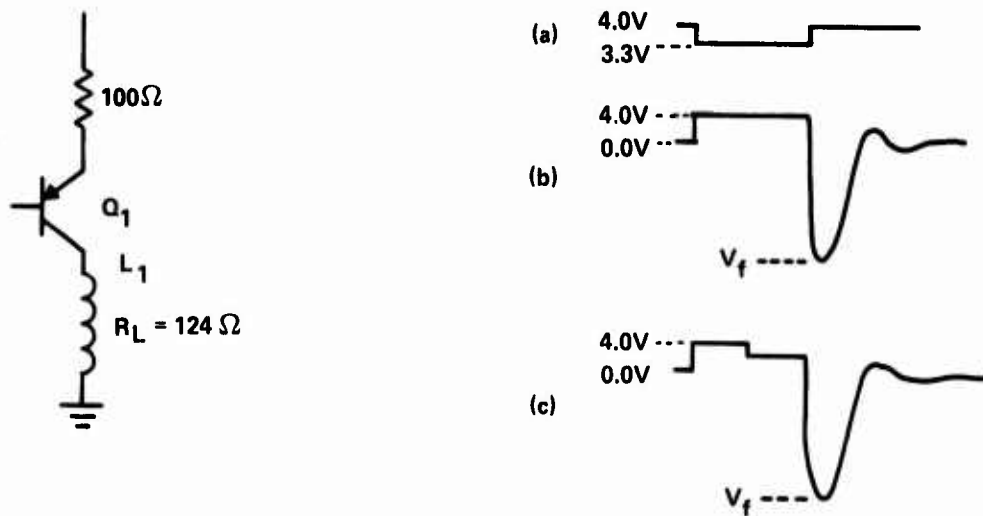


FIG. 11 CORE DRIVE CIRCUIT AND ASSOCIATED WAVEFORMS

approximately 2.2 volts as shown in figure 11c. This agrees with the earlier contention based on figure 10 that the core is not being driven to saturation in the present circuit. Moreover, analysis and measurements of the VCO circuit show that it is the pulse width and not the frequency which is being controlled by the feedback from the magnetometer output.

The low power dissipation from a core which is so easily wound is due to its not being driven into saturation. Unfortunately, the drift and noise are due in large measure to this lack of saturation. The noise figure of the closed loop magnetometer is about 500nT p-p and the drift rate is 300nT/hr.

Honeywell Voltage Controlled Oscillator.

A diagram of the Honeywell voltage controlled Oscillator (VCO) is given in figure 12. The waveforms at the output of each inverter are given in figure 13. Each inverter is composed of a complementary pair of enhancement mode MOS transistors as shown in figure 14. Q_1 is a P channel device and Q_2 is an N channel device. In inverters B, C and D terminals V_{DD} and V_{SS} are connected to the four volt regulated supply and to ground, respectively. But in inverter A, these points are connected to +4V and ground via resistors and an FET as shown in figure 12.

Let us assume that the voltage at the output terminal of inverter B has just gone low at time t_0 as shown in Figure 13. Return now to Figure 14 and let it represent inverter C. When its input goes low, transistor Q_{C2} is biased off and Q_{C1} is biased

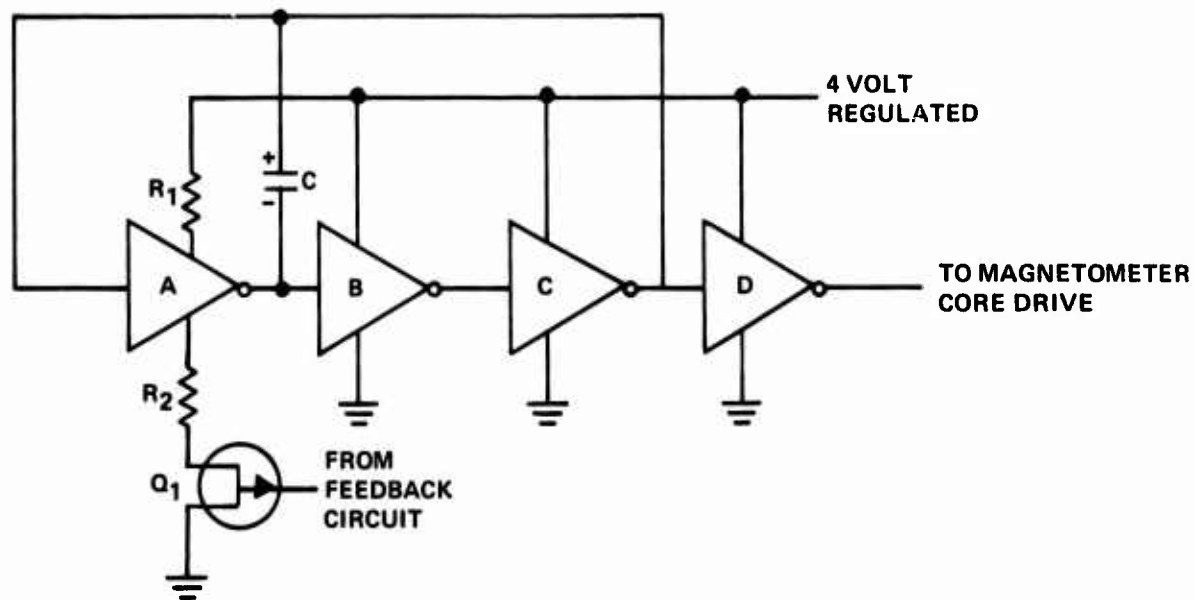


FIG. 12 HONEYWELL VOLTAGE CONTROLLED OSCILLATOR

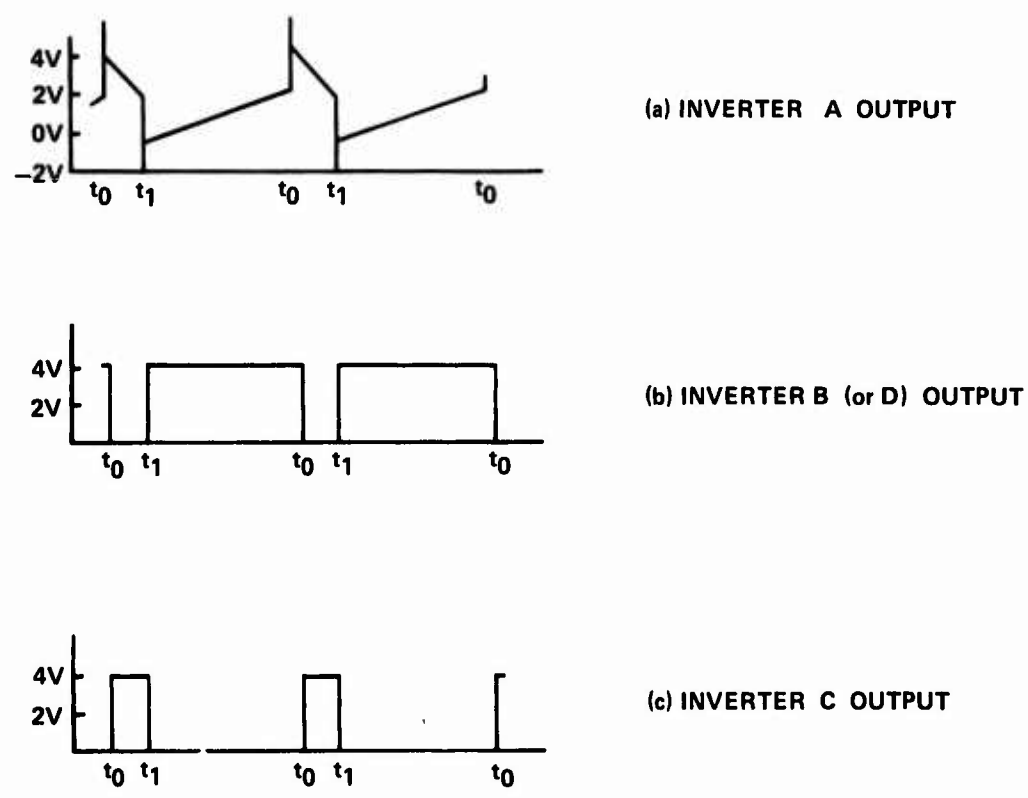


FIG. 13 VCO WAVEFORMS

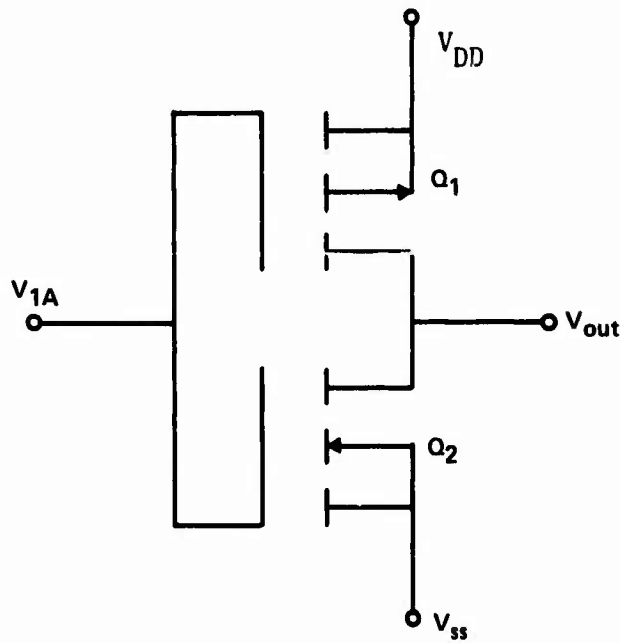


FIG. 14 INVERTER DIAGRAM

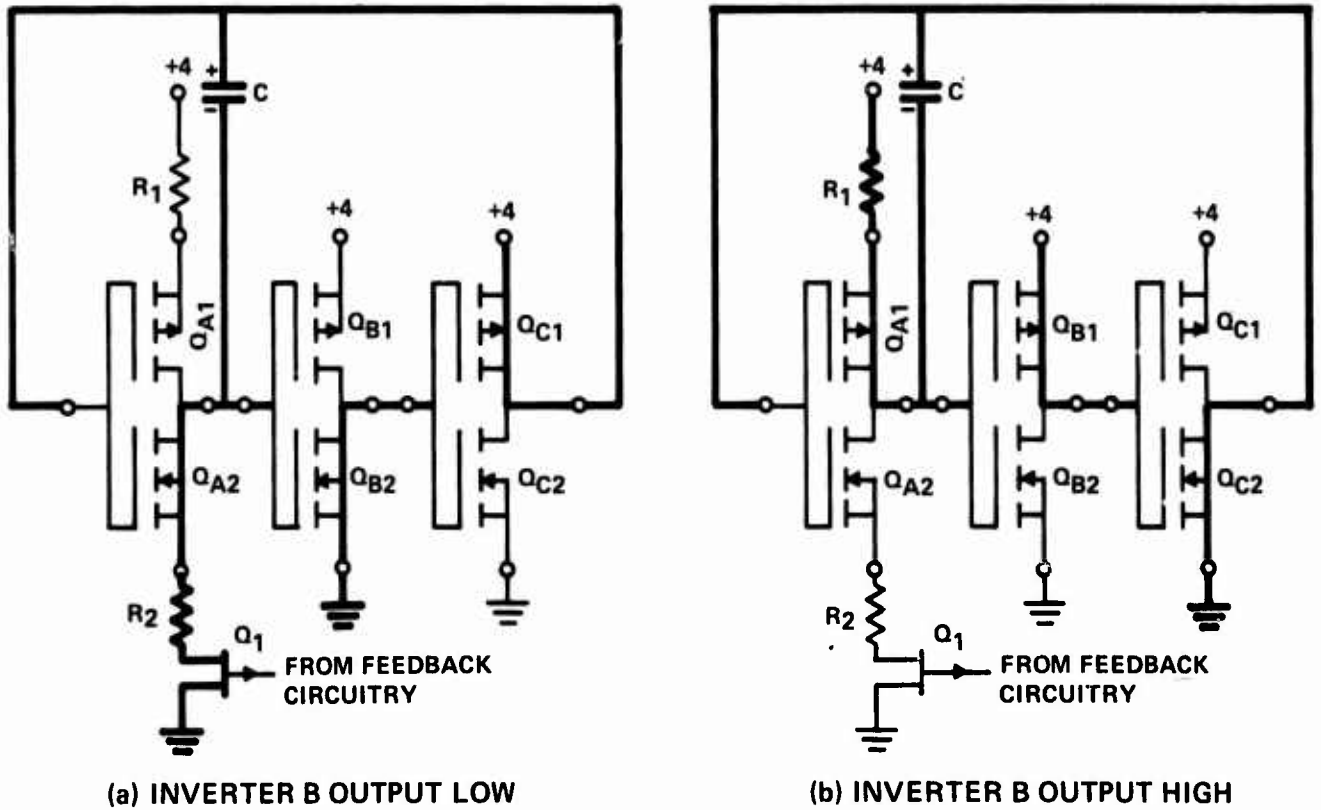


FIG. 15 VCO INVERTER ILLUSTRATIVE SCHEMATIC

on; therefore V_o equals V_{DD} . That is, the output of inverter C goes high. This voltage is applied to the input of inverter A and the positive side of capacitor C. This capacitor is non-polar and its terminals are labeled + and - in Figure 12 for reference purposes only. Since the voltage across a capacitor cannot change instantaneously for a finite current, the voltage at the input of inverter B must increase by the same amount as the voltage at the output of inverter C. But, since this would tend to cause the output of inverter B to go low, and this output has already gone low, this action just tends to reinforce the previous operation.

Now, note the spikes which appear on the inverter A output waveform at each step transition. As we will see later, the voltage at the input of inverter B will be about 2 volts when a transition takes place. Hence, the voltage across the capacitor will be about ± 2 volts at each transition point, depending on the output voltage of inverter C, and the change at the positive terminal of the capacitor will tend to drive the voltage at the negative side to either +6 or -2 volts. However, the protective diodes at the input of inverter C limit the voltage excursions effectively to +4.7 or -.7 volts.

Now let Figure 14 represent inverter A. Because a high voltage has been applied to the inverter input, Q_{A1} is off and Q_{A2} is on. There now exists a path, as shown in Figure 15a, from the 4 volt supply to ground through Q_{C1} , C, Q_{A2} , R_2 , and Q_1 . Q_1 acts like a voltage controlled resistor with a resistance of R_Q ohms. Now the

capacitor begins to discharge with a time constant $\tau = (R_2 + R_Q)C$. At time t_1 , when the voltage at the input of inverter B reaches a point in the neighborhood of one half of the supply voltage, transistor Q_{B1} and Q_{B2} will enter their linear regions. The output of inverter B will start increasing, causing the output of inverter C to start decreasing. The positive feedback around the loop composed of inverters B and C and of capacitor C will cause a rapid transition to the state where transistor Q_{B2} , Q_{C1} and Q_{A2} will be turned off and Q_{B1} , Q_{C2} and Q_{A1} will be turned on. Note that just before this transition, capacitor C will be charged to a voltage of about 2 volts. As the positive terminal of the capacitor is forced to zero, the negative terminal would be forced to -2 volts. Again, the protective diodes at the input to inverter B limit this voltage to a value of approximately -.7 volts.

After the transition, there will be a path from the positive supply terminal through R_1 , Q_{A1} , C, and Q_{C2} to ground as shown in figure 15b. The capacitor now begins to charge with a time constant $\tau_2 = R_1 C$ until the transition voltage is again reached at time t_0 . At this point regeneration due to positive feedback will cause the transition back to the originally postulated state to occur almost instantaneously and the cycle repeats.

As the voltage at the gate of the field effect transistor shown as Q_1 in figure 12 varies, the effective resistance of the channel from the drain to the source will change. As the voltage on the gate increases, the channel resistance increases which causes an

increase the time constant τ_1 . A decrease in the gate voltage of Q_1 results in decrease in τ_1 . τ_2 is a constant. During the time period t_0 to t_1 , the magnetometer core is being driven toward saturation. As can be seen from the above discussion, the drive pulse width is dependent upon the voltage applied to the gate of Q_1 in figure 12. Since the period from t_1 to t_0 is much larger than the period from t_0 to t_1 , the frequency of the VCO is virtually independent of the pulse width in its normal range of operation.

VI. DIGITAL FEEDBACK CIRCUIT

One attempted solution to the drift/stopped-vehicle-logic problem described in Ref. 1 was the replacement of the existing analog feedback circuitry shown in Figure 16 with a proposed digital feedback circuit, the block diagram of which is shown in figure 17 and the schematic of which is given in figure 18. When power to the circuit is turned on, the preset circuit sets the counter to the middle of its range and inhibits the clock for a short time. By initializing the up/down counter to its mid-point, the initial stabilization will be sped up. While not shown in figure 17, the sample control signal must be locked out until initial stabilization has been accomplished.

The magnetometer output is fed to a comparator. If the output is greater than V_{ref} , the U/D counter counts down on each positive transition of the clock. The D/A converter then applies a lower voltage to the voltage controlled oscillator (VCO) which causes an increase in the drive pulse width. The result is an increase in the magnitude of the flyback voltage and a decrease in the value of the magnetometer output voltage. Eventually the feedback will cause the voltage to fall below the 3V ref. At this point, the comparator output will go low, causing the U/D counter to count up again causing the magnetometer output to increase to just above the 3 volt point. Stabilization has now been reached. The magnetometer output will continue to change by an amount determined by the least significant bit size of the

(1) Wick, D.C., Lubke, R.A., Vehicle Detection, Phase 1, SPVD Development (U) Report No. FHWA-RD-75-18, Jan 1975 (U).

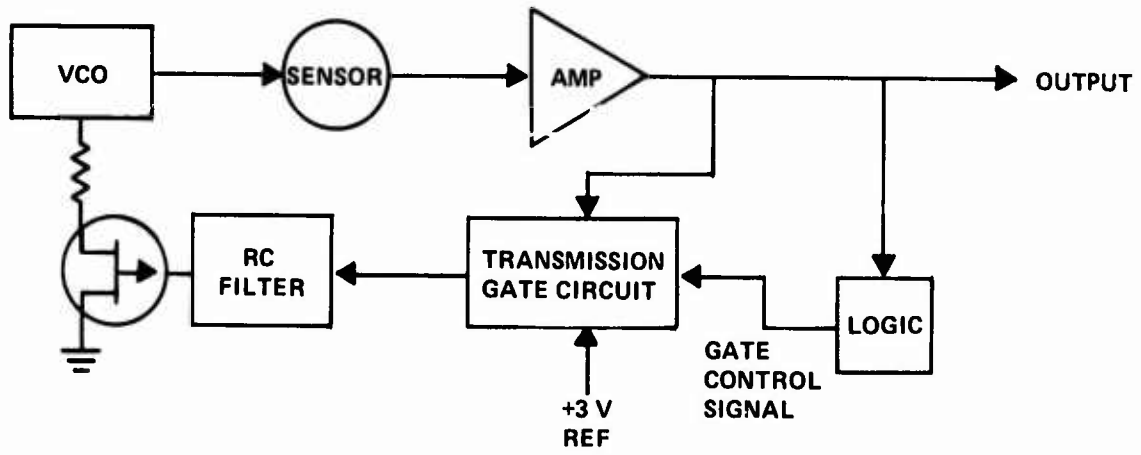


FIG. 16 BLOCK DIAGRAM, HONEYWELL ANALOG FEEDBACK CIRCUIT

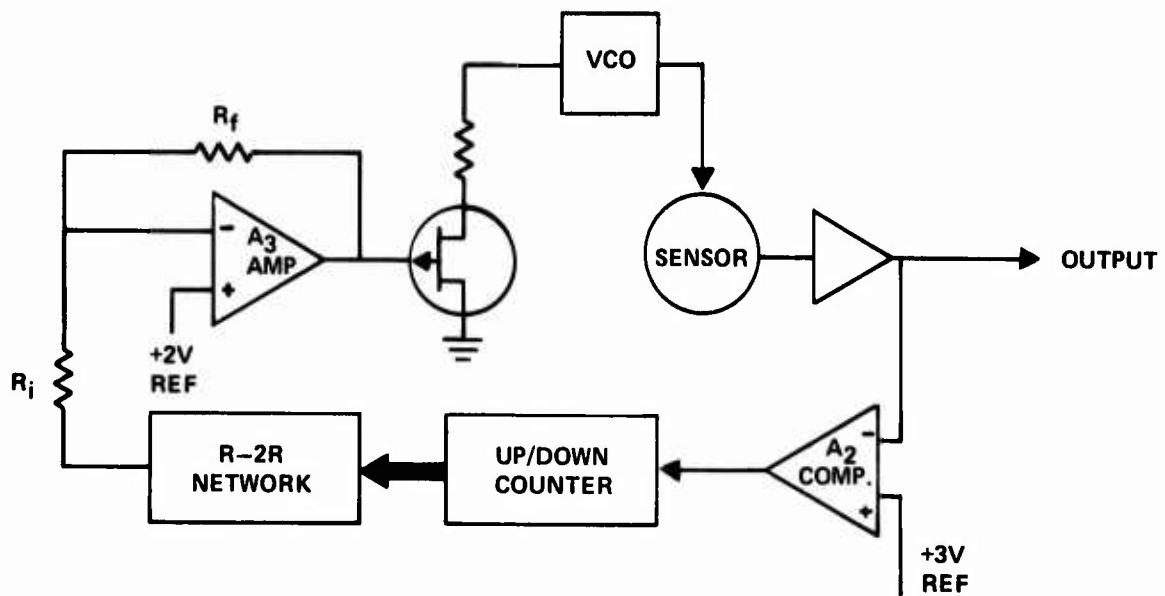


FIG. 17 BLOCK DIAGRAM, DIGITAL FEEDBACK CIRCUIT

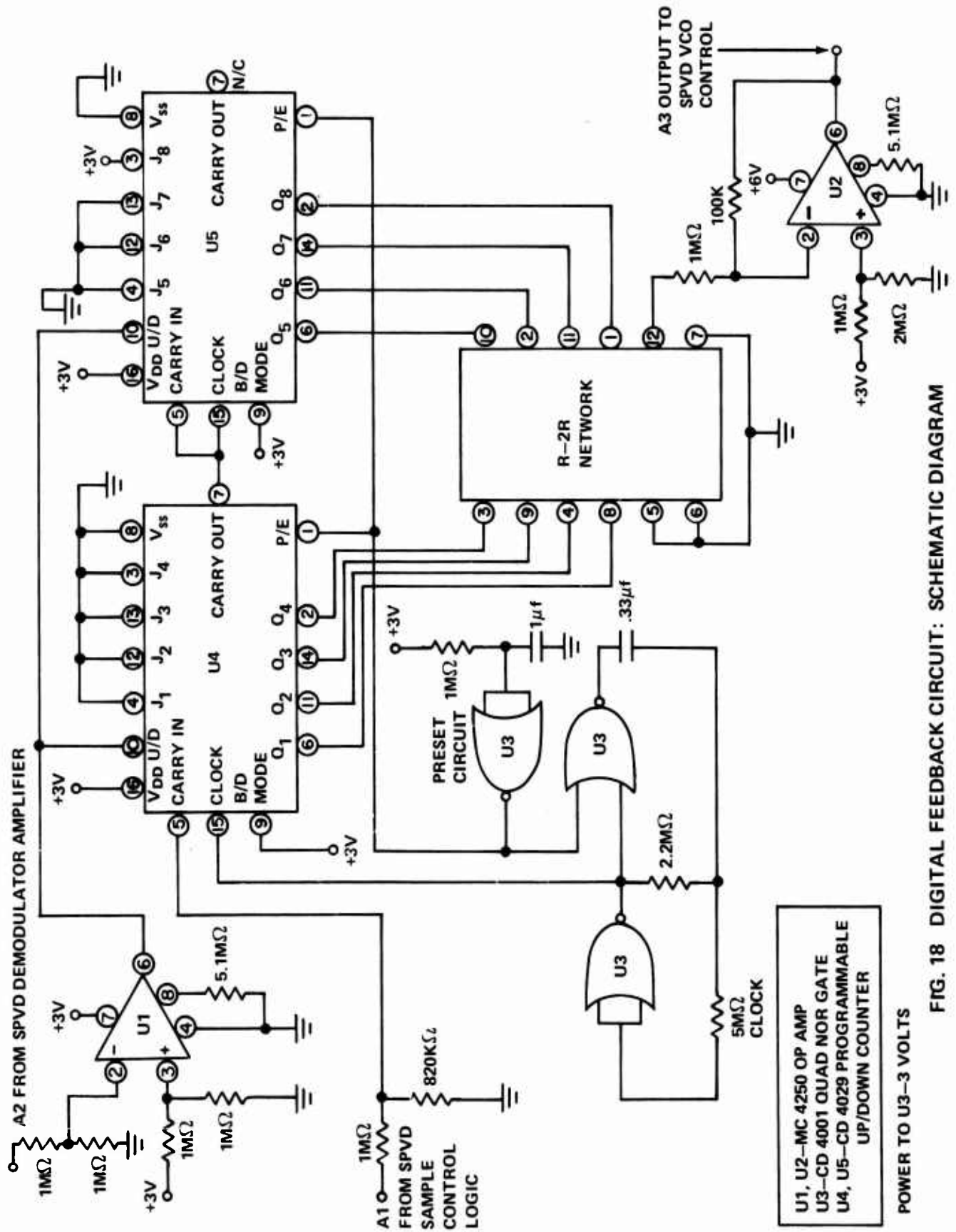


FIG. 18 DIGITAL FEEDBACK CIRCUIT: SCHEMATIC DIAGRAM

U1, U2—MC 4250 OP AMP
 U3—CD 4001 QUAD NOR GATE
 U4, U5—CD 4029 PROGRAMMABLE UP/DOWN COUNTER

POWER TO U3—3 VOLTS

digital to analog converter section of the feedback loop. The clock in the prototype unit operated at a frequency of .67Hz so that the entire range of the 8 bit converter was covered in 384 seconds. The sample control logic inhibits the operation of the counter while a vehicle is influencing the sensor. In this manner, only an ambient field change will cause a zero level shift.

The only significant power dissipation in this scheme is due to the R-2R network which is part of the digital to analog converter section. Figure 19 shows an R-2R network for a 4 bit digital to analog converter. The same principle applies to any number of bits, however. Each input V_i , where i goes from 1 to 4, is either at the positive power supply voltage V , or at ground. Voltage V_o has a value which may be expressed by the relationship

$$V_o = \frac{V_4}{2} + \frac{V_3}{4} + \frac{V_2}{8} + \frac{V_1}{16}.$$

$$\text{If } V_1 = V_2 = V_3 = V_4 = V \quad V_o = \left(\frac{1}{2} + \frac{1}{4} + \frac{1}{8} + \frac{1}{16} \right) V = \left(1 - \frac{1}{16} \right) V.$$

In general for N inputs, the maximum output voltage is

$V_o = (1 - 2^{-N})V$ and the smallest increment in output voltage is $(2^{-N}V)$ volts. When all inputs are zero, $V_o = 0$ and there is no power dissipation. It seems obvious that maximum power dissipation in any section occurs when the inputs on either side of that section impose the highest possible potential difference across that section.

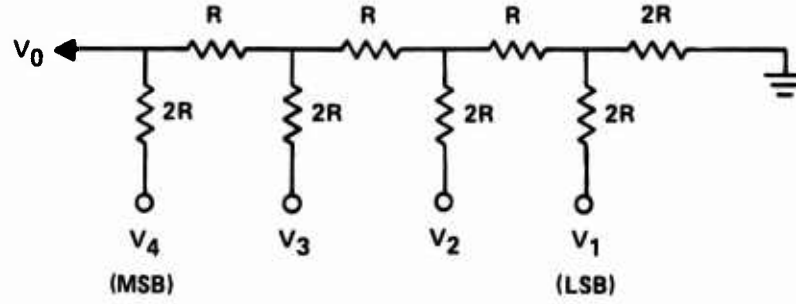


FIG. 19 FOUR BIT R-2R NETWORK

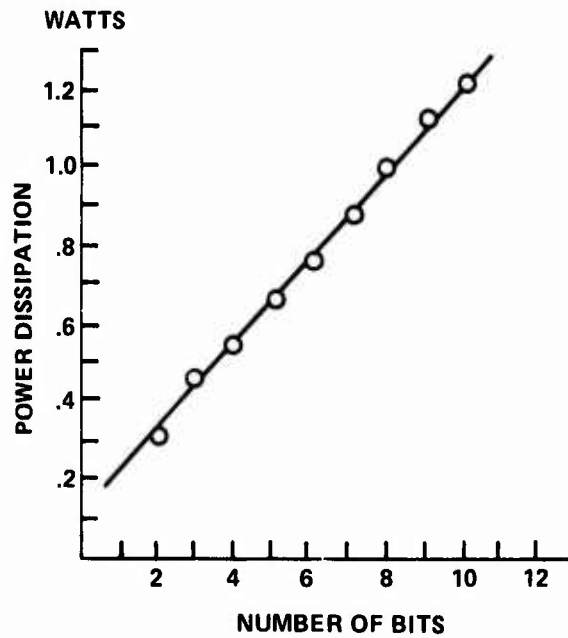


FIG. 20 POWER DISSIPATION VS NUMBER OF BITS FOR AN R-2R NETWORK

It then seems that the highest total power dissipation for the whole network occurs when the high and low voltages are imposed upon adjacent inputs. For example, in the four bit network, when $V_1 = V_3 = V$ and $V_2 = V_4 = 0$, the power dissipation should be a maximum. (The power dissipation is exactly the same for $V_1 = V_3 = 0$ and $V_2 = V_4 = V$; the directions of the currents and the signs of the potential differences are just reversed). To confirm this theory and to calculate the value of the maximum power dissipation for a network of n bits, a computer program was written and run on a Hewlett-Packard 9820A calculator. The program calculated the power dissipation for half of the possible input conditions (the other half were mirror image states with identical power dissipations) and gave as an output the value of the maximum dissipation and the input voltage state for which it occurred. The program assigned a value of 1 ohm to R and 1 volt to V to facilitate scaling. The results are given in table 3 and plotted in figure 20. As can be seen in figure 20 the power dissipation is linear with respect to the number of bits. Therefore this figure can be used to determine the maximum power dissipation for any number of bits. Or, alternatively a formula which gives a close approximation for $N \geq 4$, and which was determined by linear regression, can be used. It is

$$P.D._{\max} = (.104 + .112N) \text{ watts.} \quad (\text{Eq. 1})$$

TABLE 3

MAXIMUM POWER DISSIPATION FOR AN N-BIT R-2R NETWORK WHERE
R = 1Ω , V = 1 VOLT

<u>NUMBER OF BITS</u>	<u>POWER DISSIPATION (WATTS)</u>
2	.313
3	.453
4	.551
5	.669
6	.777
7	.889
8	1.000
9	1.110
10	1.220

The coefficients of the higher order terms in equations of higher degree were so small, that this equation is the best, except for values of $N \leq 3$.

For values of V and R which differ from one volt and one ohm,

$$PD_{\max} = \frac{V^2}{R} PD_{\max}$$

where P.D. max is the value of the power dissipation from table 3 or calculated using eq. 1. For the 8 bit network used in the digital feedback network installed in the SPVD at NSWC, the resistance R had a value of 50K ohms and the input voltage was 3 volts. Therefore, the power dissipation was

$$PD_{\max} = (1.00) \left(\frac{3^2}{5 \times 10^4} \right) = 180 \mu W$$

The number of bits needed is a function of the dynamic range and the resolution required, and can be determined by the equation

$$N = \frac{\ln \left(\frac{\text{Range}}{\text{Resolution}} \right)}{\ln 2}$$

where the range and resolution are expressed in the same units. For a dynamic range of 100,000 nanotesla and a resolution of 100 nanotesla

$$N = \frac{\text{Ln}\left(\frac{100000}{100}\right)}{\text{Ln } 2} = \frac{6.91}{.693} = 9.97$$

Therefore, N must be at least 10 bits. As the number of bits is increased, either the expense of the R-2R network is greatly increased or the value of R must be decreased. But, decreasing the value of R increases the power dissipation as was shown earlier.

In the digital feedback network constructed and tested for inclusion in the SPVD, only 8 bits were used. The R-2R network was a TRW ceramic substrate, 12 pin integrated circuit where the value of R was 50K Ω . The model was constructed to prove the feasibility of the scheme and either the range or the resolution of the circuit shown in figure 17 would not be adequate for a final design. Another 4-bit up/down counter and utilization of all sections of the R-2R network will be required in the final design.

When the up/down counter changed by one bit, the output, labeled A3 in figure 17, from the digital feedback network changed by 10mV. This in turn caused a 120 mV change in the output of the magnetometer amplifier. This magnetometer output is labeled A2 in figure 17 and is shown as the input to the digital feedback network. For an ambient magnetic field change of 1680 gammas, A2 would also change by 120 mV. The range of the device tested was

greater than $\pm 400,000$ nT. By reducing resistor R1 from a value of $100K\Omega$ to $5K\Omega$, the step size of output A_2 from the magnetometer was reduced to 84 nT while the range was reduced to $\pm 21,000$ nT. However, this range is more than adequate to compensate for the variation expected due to temperature variations and other factors. Temperature tests must still be run to verify this. Also, by going to 10 bits, the range can be extended to 84,000 nT.

Honeywell feedback scheme

While attempting to incorporate the above digital feedback scheme into the present SPVD, certain difficulties arose. Chief among these was that as long term drift was minimized, the stopped vehicle presence problem was maximized. The existing SPVD logic also resulted in the failure of the Brown magnetometer, as described earlier, to cure the presence problem. In order to simulate a magnetometer with zero drift, a variable power supply was used in place of the actual magnetometer amplifier. The vehicle presence problem was now so severe that anytime a "vehicle" stopped for more than 5.6 seconds (nominal time), a trailing edge pulse was never generated by that "vehicle." At this point an analysis of the system logic seemed to be in order. The results of this investigation will be given below.

With the present feedback circuit, as shown in figure 16, the feedback is normally controlled by the sensor output. However, control is transferred to the 3 volt reference signal while a moving vehicle is influencing the sensor; that is, while the field

remains above 3000 nT after having attained a magnitude greater than 7000 nT. If the magnetometer output is still above 3000 nT after 5.6 seconds (nominal), the logic switches control back to the magnetometer output, supposedly allowing the magnetometer to re-zero itself.

This is one fundamental problem with the present logic/feedback arrangement. The feedback loop has a time constant which is long with respect to the time it takes a slowly moving vehicle to traverse the sensor locations. This allows correction of long term drift while minimizing attenuation of vehicle signals. The logic, however, requires that the magnetometer be rapidly zeroed after a stopped vehicle has been detected; but the same long time constant feedback loop is used for this purpose. If the magnetometer has not been adequately zeroed by the time the vehicle leaves, a leading edge pulse will not reset the sample control logic and the trailing edge pulse cannot be generated. It will take another vehicle to generate the leading edge pulse required to reset the logic and generate a trailing edge pulse.

The term "adequately zeroed" in the last paragraph must be explained. It means that the output level of the magnetometer must shift by such an extent that when the vehicle moves away a reverse field of 7000 nT in the vertical direction is detected. To see why this is so, a further look at the logic, the block diagram for which is shown in figure 21, and at the feedback is required. When a signal of 7000 nT in the vertical direction

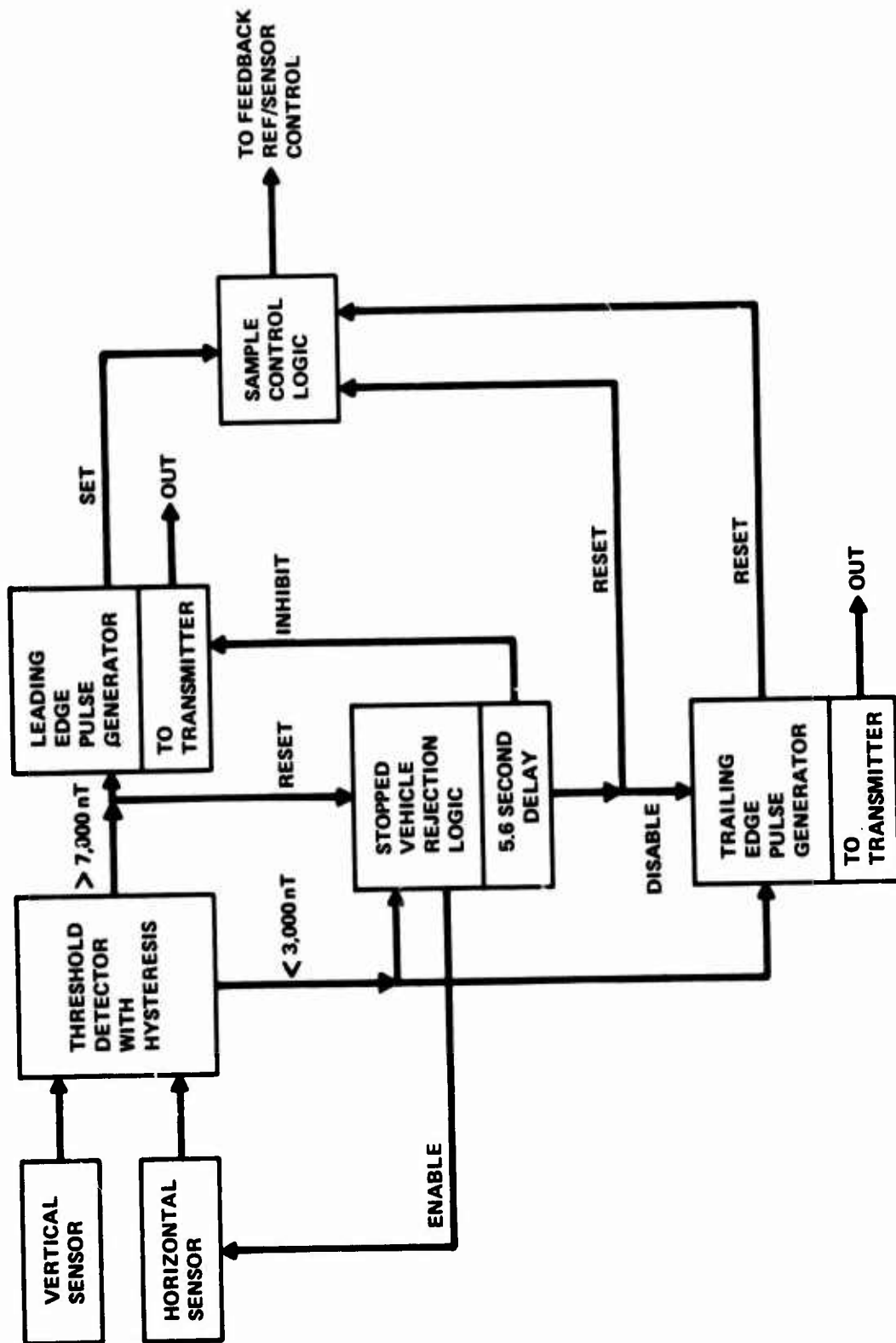


FIG. 21 SPVD LOGIC BLOCK DIAGRAM

is detected, the output from the leading edge pulse generator to the sample control logic (SCL) switches the feedback control from the magnetometer output to the reference. An output from the stopped vehicle rejection logic (SVRL) simultaneously enables the horizontal magnetometer output. After 5.6 seconds have elapsed, a second output from the SVRL disables the trailing edge generator and resets the SCL. A third output from the SVRL inhibits the generation of a leading edge output to the transmitter and SCL. When both the vertical and horizontal magnetometers simultaneously indicate fields below 3000 nT, the output from the SVRL to the horizontal magnetometer inhibits this channel. All other outputs remain the same. This is true whether the output levels decrease due to rezeroing or due to the vehicle moving away. In order for a trailing edge pulse to be generated, the vertical channel must detect a signal change great enough to cause the 7000 nT threshold level to be crossed. Due to effects to be described later, this threshold level will be opposite in sign to that initially generated if the same vehicle which produced the leading edge pulse sent to the transmitter is to also generate the trailing edge pulse. But, if the original vehicle has already moved away without generating a trailing edge pulse, a subsequent vehicle can cause the 7000 nT level to be crossed. It doesn't matter which polarity the signal actually has as it is full wave rectified. This second crossing of the 7000 nT threshold resets the SVRL to allow generation of a trailing edge pulse. Again, another SVRL output enables the

horizontal magnetometer output. Now, provided that both magnetometers indicate field levels less than 3000 nT concurrently within 5.6 seconds of the 7000 nT vertical threshold crossing, a trailing edge pulse will be generated. Should the 5.6 second time again be exceeded, the inhibit cycle will start all over and a trailing edge pulse may still not be generated.

Let us return to the feedback loop time constant. It has been shown that it is long with respect to vehicle transit times of moving vehicles. Now let us consider a typical magnetometer output signal, as shown in figure 22, due to a vehicle which has stopped over the sensor. The time constant of the present feedback loop is about 300 seconds due to the values of components in the RC filter shown in figure 16. The magnetometer output increases until, at time t_0 , the threshold detector actuates. The field level due to the source rises to a maximum value of α . The vehicle stops for at least 5.6 seconds so that at $t_1 = t_0 + 5.6$ sec, the stopped vehicle rejection logic is triggered. During the period from t_0 to t_1 , the feedback is being controlled by the reference voltage rather than by the magnetometer signal voltage. This will cause the delay times to be developed to be slightly different from those which actually would occur. This and other second order effects will be neglected in this analysis. The principles remain the same, however, and the results agree with the observations in a qualitative manner although controlled quantitative measurements were not taken.

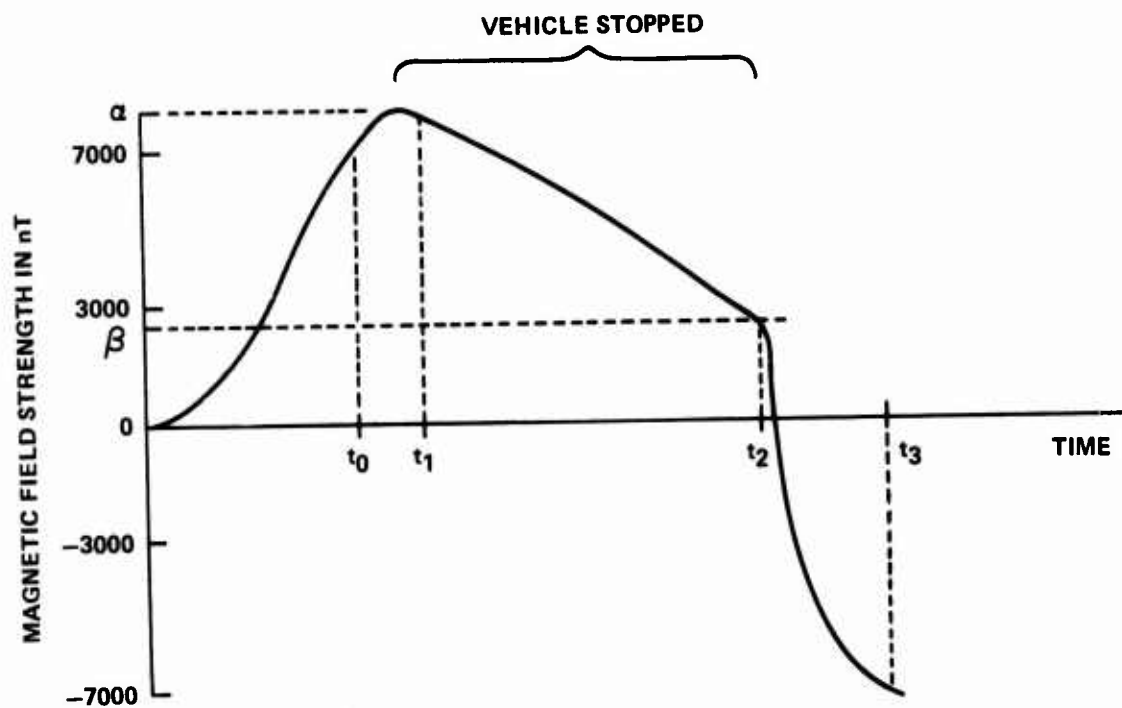


FIG. 22 MAGNETOMETER OUTPUT VS STOPPED VEHICLE PRESENCE TIME

While the vehicle is stopped, the net field sensed by the core will decrease. The feedback will cause the field due to the drive pulse to change to compensate for the field due to the vehicle. This decrease can be expressed as an exponential so that

$$\beta = \alpha e^{-\left(\frac{t_2 - t_0}{\tau}\right)} \quad (\text{Eq. 2})$$

where τ is the 300 second constant of the feedback loop. At time t_2 the vehicle starts to move away. To ensure that the threshold is crossed, the level reached at time t_3 must be -7000 nT. But, the change in field due to a leaving vehicle must have the same magnitude and opposite sign as the field change caused by that vehicle's approach. Otherwise the ambient field must be capable of some "memory." Therefore, $\alpha = \beta + 7000$. Now we can solve for $t_2 - t_0$ in terms of α . If a vehicle stops for 5.6 seconds, there is a minimum time it must remain stopped in order to generate a trailing edge pulse. If we insert the relationship $\alpha = \beta + 7000$ into equation 2, we find

$$(t_2 - t_0) = \tau \text{Ln} \frac{\alpha}{\alpha - 7000} \quad (\text{Eq. 3})$$

which gives the minimum stop time required for a vehicle which produces a peak magnetic output signature of α nanoteslas. Table 4 gives a list of minimum stop times for a vehicle of peak signature

TABLE 4

MINIMUM TIME A VEHICLE MUST REMAIN STOPPED, IF IT STOPS
FOR AT LEAST 5.6 SECONDS, AS A FUNCTION OF PEAK MAGNETIC
FIELD SIGNATURE

<u>PEAK MAGNETIC SIGNATURE (nT)</u>	<u>MINIMUM STOP TIME (Seconds)</u>
>378,511	none
350,000	6.1
200,000	10.7
100,000	21.8
50,000	45.2
20,000	129.0
10,000	361.0
8,000	623.0
7,050	1490.0

α as computed by eq. 3. It must be remembered that the values given in Table 4 were computed using an equation developed with the aid of many approximations and the actual measured times may vary considerably from these.

In order to alleviate this stopped vehicle problem, two solutions using the digital feedback scheme are readily apparent. First, the present logic could be retained and the clock could be speeded up when a stopped vehicle has been detected. This solution would facilitate initial zeroing and eliminate any worry about a large vehicle or other magnetic source stopping near the roadway and keeping the field at the sensor above the low threshold. The second solution would be to stabilize the sensor and redesign the logic to eliminate the need for a stopped vehicle detection. If it is assumed that large masses of magnetic material will never be placed near the sensor for long periods of time, the second alternative is the more attractive of the two, since the first would require an increased range and therefore more power consumption.

Digital Feedback for Brown Magnetometer

In order to eliminate the temperature dependence and other long term drift described in a previous section of this report, digital feedback can also be used with the Brown Magnetometer. To determine the feasibility of this method, the digital feedback section designed to replace the analog feedback to the Honeywell sensor was modified to work with the Brown Sensor. The resultant, modified circuit is shown schematically in figure 23 and by a block

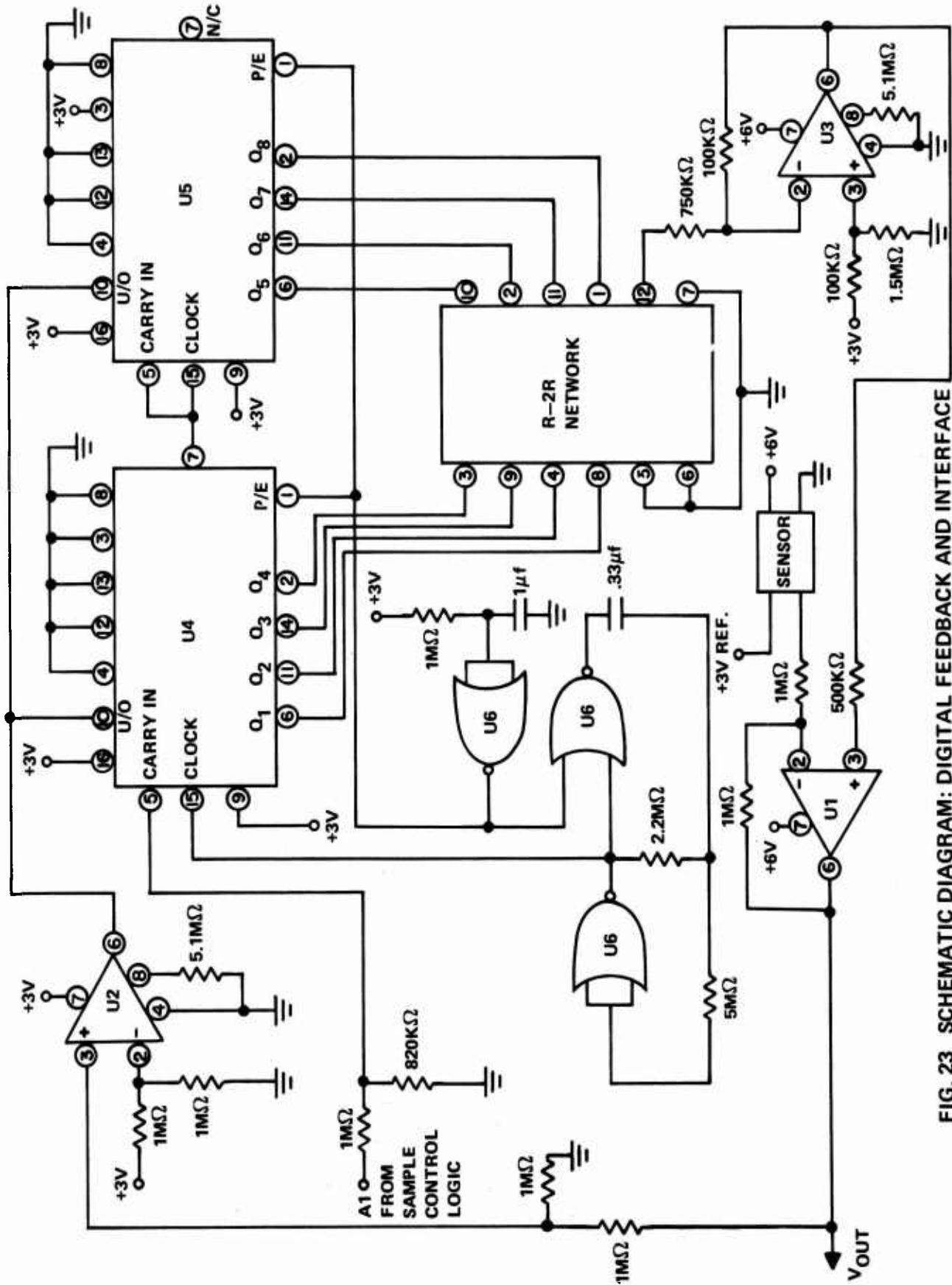


FIG. 23 SCHEMATIC DIAGRAM: DIGITAL FEEDBACK AND INTERFACE CIRCUIT FOR USE WITH THE BROWN MAGNETOMETER

diagram in figure 24. The output of the Brown Magnetometer is processed by a unity gain amplifier and, in zero ambient field, V_{out} is 3 volts. If either an ambient field change or drift in the electronics causes V_{out} to drift above V_{ref} , which in this case is 3 volts, the output of comparator U2 goes high and causes the up/down counter (U/D counter) to count up. This causes the output voltage from the R-2R network to increase, which in turn produces a decrease in the output voltage of U3, which acts as the reference voltage for amplifier U1. This produces a decrease in V_{out} until V_{out} is below the 3 volt reference.

When the field changes rapidly and attains a magnitude of 7000 nT, the SPVD assumes that this field change is due to a vehicle and an inhibit signal is generated to turn off the U/D counter until the field again drops below 3000 nT in both the Horizontal and vertical channels. This inhibit signal can be obtained from the first inverter in the anti-chatter circuit of the SPVD.

The circuit constructed in accordance with figure 23 had a measured range of 10^{-4} tesla and a minimum step size of 428 nT. No temperature tests were run because of time limitation.

It may be desirable to make two changes in the final version, in addition to adding the two extra bits to the D/A converter. The first change is the addition of a provision for rezeroing the output if it remains locked up for some arbitrary period. The other is to increase the gain of the buffer amplifier, U1 in figure 23, so that the output voltage will be approximately 14.7 volts per Oersted,

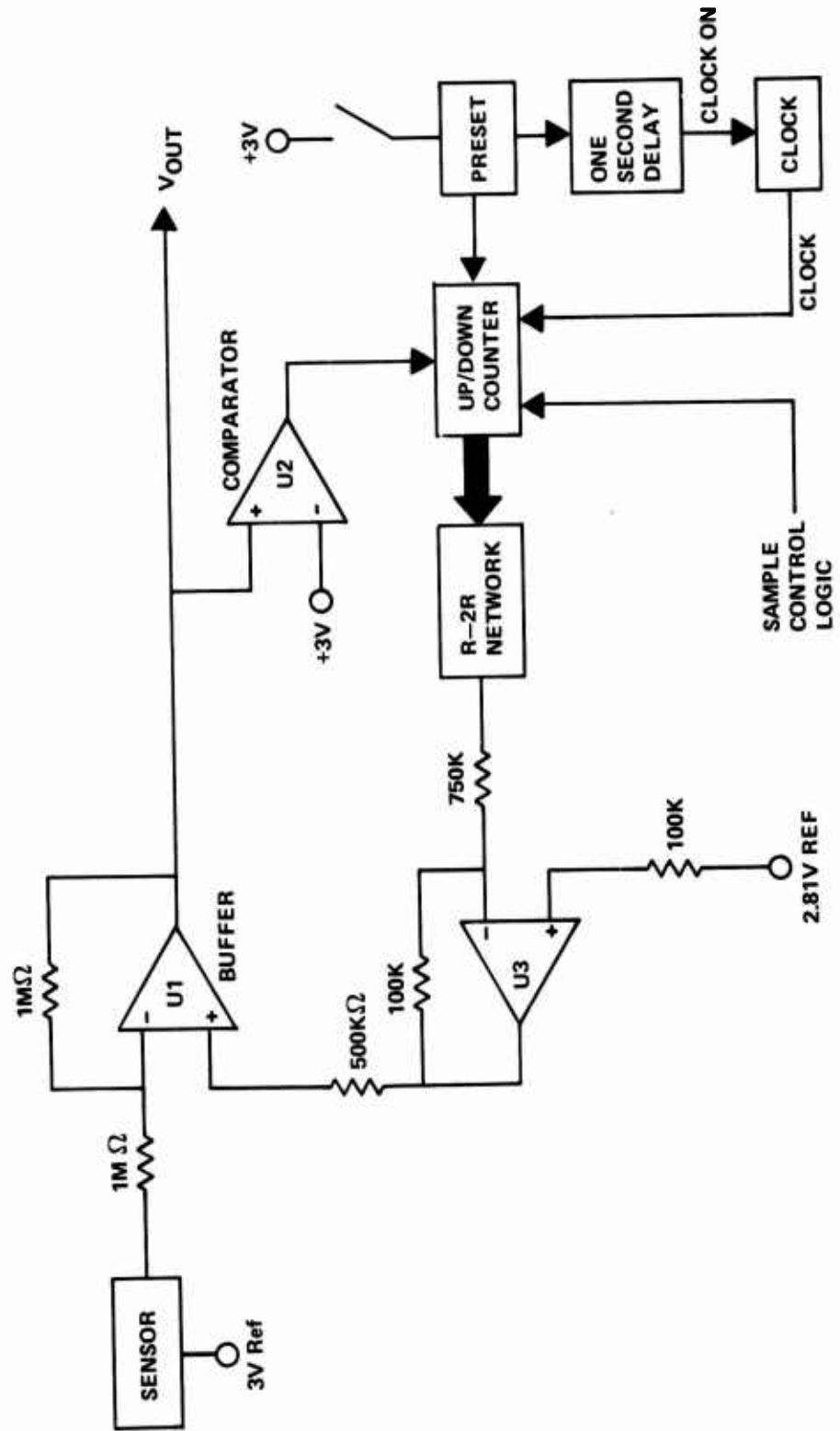


FIG. 24 BLOCK DIAGRAM OF DIGITAL FEEDBACK AND INTERFACE CIRCUITS FOR USE WITH THE BROWN MAGNETOMETER

which is the conversion constant of the Honeywell circuit. This would necessitate only a change in the values of the components in the digital feedback loop in addition to the feedback resistor across U1.

VII. DISCUSSION

Both the Brown and Honeywell type ring core magnetometers were investigated for performance, low power and low cost goals of the SPVD. The main cost of the Brown Magnetometer is in core winding. This may be lessened if a core with less magnetic material is used ($> L/D$), but the dynamic range and sensitivity may be adversely affected with the fewer windings used. The present sensor, using a 10 wrap core has a substantial safety factor, i.e. large dynamic range, in case it is positioned near reinforcing rods or source of high fields. Although further development should improve performance and cost, the present sensor appears adequate for the SPVD. Medium Volume (100) magnetometer unit cost is estimated at \$40.00, including circuit board, windings, assembly and components.

The Honeywell sensor, if used with a digital feedback loop for sensor stabilization would probably be adequate for the SPVD. However, the component cost advantages that might be realized if used instead of the Brown magnetometer, still would not match the performance as tabulated in table 2.

The digital feedback loop when used to stabilize the Brown magnetometer with respect to long term and thermal drift, appears to be the main solution to the vehicle presence problems associated with the present SPVD. In order to utilize the developed sensor, the sensor logic will be modified so that the leading and trailing pulses will activate the telemetry transmitter reliably. The only

large cost encountered in this design is the R-2R resistor networks (\approx \$25 each) required for each magnetometer axis digital feedback loop. It is anticipated that per unit costs will drop in quantity.

DISTRIBUTION

	Copies
Federal Highway Administration Office of Research, Traffic Systems Division Washington, D.C. 20590 Attn: P. Mills	40
Naval Sea Systems Command Washington, D.C. 20360 SEA 0333C (F. Henry) SEA 0342 (W. Welsh)	1 1
David W. Taylor Naval Ship R & D Center Magnetic Fields Branch Annapolis, MD. 21404 Attn: D. G. Everstine B. R. Hood	1 1
Office of Naval Research Washington, D.C. 20360 Attn: R. F. Obrochta (ONR-463)	1
Defense Documentation Center Cameron Station Alexandria, Virginia 22314	2

TO AID IN UPDATING THE DISTRIBUTION LIST
FOR NAVAL SURFACE WEAPONS CENTER, WHITE
OAK LABORATORY TECHNICAL REPORTS PLEASE
COMPLETE THE FORM BELOW:

TO ALL HOLDERS OF NSWC/WOL/TR 76-58
by J. F. Scarzello, Code WR-43

DO NOT RETURN THIS FORM IF ALL INFORMATION IS CURRENT

A. FACILITY NAME AND ADDRESS (OLD) (Show Zip Code)

NEW ADDRESS (Show Zip Code)

B. ATTENTION LINE ADDRESSES:

C.

REMOVE THIS FACILITY FROM THE DISTRIBUTION LIST FOR TECHNICAL REPORTS ON THIS SUBJECT.

D.

NUMBER OF COPIES DESIRED _____

ATTENTION: CODE WR-43
COMMANDER
NAVAL SURFACE WEAPONS CENTER
WHITE OAK, SILVER SPRING, MARYLAND 20910

DEPARTMENT OF THE NAVY
NAVAL SURFACE WEAPONS CENTER
WHITE OAK, SILVER SPRING, MD. 20910
OFFICIAL BUSINESS
PENALTY FOR PRIVATE USE, \$300

POSTAGE AND FEES PAID
DEPARTMENT OF THE NAVY
DOD 316



THIS REPORT HAS BEEN DELIMITED
AND CLEARED FOR PUBLIC RELEASE
UNDER DOD DIRECTIVE 5200.20 AND
NO RESTRICTIONS ARE IMPOSED UPON
ITS USE AND DISCLOSURE.

DISTRIBUTION STATEMENT A

APPROVED FOR PUBLIC RELEASE;
DISTRIBUTION UNLIMITED.